Numerical investigation of wave-plus-current induced scour beneath two submarine pipelines in tandem

Li, Yuzhu; Ong, Muk Chen; Fuhrman, David R.; Larsen, Bjarke Eltard

Published in:
Coastal Engineering

Link to article, DOI:
10.1016/j.coastaleng.2019.103619

Publication date:
2020

Document Version
Publisher's PDF, also known as Version of record

Coastal Engineering 156 (2020) 103619

Contents lists available at ScienceDirect

Coastal Engineering

journal homepage: http://www.elsevier.com/locate/coastaleng

Numerical investigation of wave-plus-current induced scour beneath two submarine pipelines in tandem

Yuzhu Li [a], Muk Chen Ong [a,*], David R. Fuhrman [b], Bjarke Eltard Larsen [b]

[a] Department of Mechanical and Structural Engineering and Materials Science, University of Stavanger, N-4036, Stavanger, Norway
[b] Section of Fluid Mechanics, Department of Mechanical Engineering, Technical University of Denmark, DK-2800, Kongens, Lyngby, Denmark

ARTICLE INFO

Keywords:
Scour
Pipelines in tandem
Wave and current
Turbulence modeling

ABSTRACT

Two-dimensional (2D) local scour beneath two submarine pipelines in tandem under wave-plus-current conditions is investigated numerically. A fully-coupled hydrodynamic and morphologic model based on unsteady Reynolds-averaged Navier-Stokes (URANS) equations with the $k-\omega$ turbulence closure is applied. The model is validated against existing experimental measurements involving live-bed scour beneath a single pipeline and beneath two pipelines in tandem, respectively. The model is then employed to simulate scour beneath two tandem pipelines under wave-plus-current conditions for a variety of Keulegan-Carpenter (KC) numbers and relative current strengths. Horizontal gap ratios (the horizontal gap distance between two pipelines divided by the pipeline diameter) ranging from 1 to 4 are modelled. It is found that for conditions involving waves plus a low-strength current, the scour pattern beneath two pipelines behaves like that in the pure-wave condition. Conversely, when the current has equal strength to the wave-induced flow, the scour pattern beneath two pipelines resembles that in the pure-current condition. It is also observed that in the pure-wave condition the equilibrium scour depth beneath each pipeline is affected by both KC and the horizontal gap ratio, except for $KC = 5.6$. For such a small KC, the horizontal gap ratio has insignificant influence on the equilibrium scour depth, since vortex shedding does not occur. When the current strength relative to the waves is low, the scour development beneath the upstream and the downstream pipelines are similar. However, when the current has equal strength to the waves, the scour development beneath the downstream pipeline has a different pattern to that upstream. Namely, smaller horizontal gap ratios result in delayed scour beneath the downstream pipeline.

1. Introduction

In the submarine environment hydrodynamic loads from waves and currents can act on submarine pipeline systems simultaneously. Once pipelines are installed on the seabed, the local flow patterns will be changed and the sediment transport capability can be increased. Significant local scour has been observed during surveys of submarine pipelines in service. The development of scour beneath such pipelines can cause free spanning of the pipeline, which can increase structural fatigue and damage. To predict the local scour under pipelines, research has been conducted mainly in three forms: (1) empirical models based on experimental data, e.g., Mao (1986), Sumer and Fredsøe (1990, 1996), (2) numerical models based on potential flow theory, e.g., Chao and Hennessy (1972), Chiew (1991), Li and Cheng (1999), and (3) numerical models capable of describing turbulent flows, e.g., Brørs (1999), Li and Cheng (2000), Liang et al. (2005), Fuhrman et al. (2014) and Larsen et al. (2016).

Mao (1986) performed a series of experiments involving scour beneath pipelines under a variety of flow conditions. It was found that the equilibrium scour depth divided by the pipeline diameter S_e/D is a weakly varying function of the Shields parameters θ. An empirical formula for the equilibrium scour depth in the live-bed regime based on Mao (1986)'s experimental measurement was established by Sumer and Fredsøe (2002). In the clear-water regime, the variation in scour depth with θ was large, and therefore no simple formula exists. For scour in waves, Sumer and Fredsøe (1990) investigated the variation of the scour depth with the Keulegan–Carpenter number (KC) and found that S_e/D is a function of $\sqrt{KC}$ in the live-bed regime. In the case of combined waves and currents, Sumer and Fredsøe (1996) conducted experiments covering a wide range of wave-plus-current conditions. It was found that the scour depth may increase or decrease in wave-plus-current conditions relative to pure-wave conditions, depending on both KC and the current velocity relative to the wave-induced near-bed orbital velocity.

* Corresponding author.
E-mail address: muk.c.ong@uis.no (M.C. Ong).

https://doi.org/10.1016/j.coastaleng.2019.103619
Received 16 April 2019; Received in revised form 6 October 2019; Accepted 7 December 2019
Available online 14 December 2019

Nomenclature

a	Non-dimensional coefficient for bed load particle moving velocity
b	Reference level of suspended sediment concentration
c	Suspended sediment concentration
c_b	Reference concentration of suspended sediment
c_D	drag coefficient
d	median grain diameter
D	Pipeline diameter
D_s	Sediment deposition rate
E_s	Erosion rate
F_i	External body force driving the flow
h	Computational domain height
h_b	Bed height
k	Kinetic energy of turbulent fluctuations per unit mass
m	Relative current strength
n	Porosity
q_B	Bed load transport rate
R	Reynolds number
S_0	Initial scour hole depth
S_e	Equilibrium scour depth
S_{ij}	Mean strain rate tensor
t	Time in second
T_w	Wave period
u_i	Mean velocities in x_1, x_2, x_3 directions
U_B	Bed load particle moving velocity
U_f	Friction velocity
U_{fc}	Friction velocity of the pure-current flow
U_m	Near-bed orbital velocity amplitude of the oscillating flow
w_s	Settling velocity
x_i	Cartesian coordinates
$\alpha,\beta,\beta^*,\sigma,\sigma^*,\sigma_{d0},C_{lim}$	Constant coefficients for the present $k-\omega$ model
β_s	Ratio factor for sediment particle diffusivity and eddy viscosity
δ_{ij}	Kronecker delta
γ	Slope angle of the bed
μ_d	Dynamic friction coefficient
μ_s	Static friction coefficient
ν	Fluid kinematic viscosity
ν_T	Eddy viscosity
ω	Specific dissipation rate
ω_s	Sediment settling velocity
ρ	Density of the fluid
ρ_s	Density of the sediment grains
τ_{ij}	Reynolds stress tensor
θ	Shields parameter
θ_c	Critical Shields parameter for a slope bed
θ_{c0}	Critical Shields parameter for a horizontal bed
θ_{cw}	Far-field Shields parameter for the wave-plus-current flow
θ_m	Mean Shields parameter for the wave-plus-current flow
θ_w	Maximum Shields parameter for the oscillating flow

In addition to experimental studies, early attempts on numerically modelling the scour beneath pipelines were based on potential flow theory, according to Sumer (2007) and Sumer (2014). The studies of Chao and Hennessy (1972), Chiew (1991) and Li and Cheng (1999) could predict the maximum scour depth and the upstream slope. However, the potential flow theory cannot capture the flow separation and formation of lee-wake vortices, which are responsible for a more gentle downstream slope (Sumer and Fredsøe, 2002).

More recent attempts at the numerical modelling of scour beneath submarine pipelines have been based on the complete Navier-Stokes equations, with turbulence modelling in the form of either Reynolds-averaged formulations or Large Eddy Simulations (LES). Li and Cheng (2000, 2001) have used LES to model the local scour beneath a pipeline. Their studies modelled the scour development using local amplification of the bed shear stress, but they did not model the sediment transport process. Brørs (1999) used a $k-\varepsilon$ turbulence model to solve the Reynolds-averaged Navier-Stokes (RANS) equations and established a numerical model to describe the flow, sediment transport and morphology in steady currents. However, as demonstrated in the work of Lee et al. (2016), the $k-\varepsilon$ turbulence model cannot reproduce the vortex shedding so that the lee-wake erosion stage cannot be properly modelled. Liang and Cheng (2005) carried out a numerical study of scour in waves and used a $k-\omega$ turbulence model for closure. The $k-\omega$ turbulence model is able to capture the vortex shedding. Fuhrman et al. (2014) likewise used a $k-\omega$ turbulence model (Wilcox, 2006, 2008) to solve the unsteady RANS equations and simulated both the scour development, as well as backfilling, that occurs for various *KC*. Larsen et al. (2016) simulated the scour around a pipeline in wave-plus-current conditions with the same model. In their work, similar trends as seen in Sumer and Fredsøe (1996) were obtained for the variation of the equilibrium scour depth with the relative current strength. Bayraktar et al. (2016) also utilized the model to simulate wave-induced backfilling from a current generated scour hole and achieved equilibrium depths and time scales in line with their experimental results.

Extensive studies have been performed to predict the scour around a single submarine pipeline, though pipelines may also be laid in tandem. For example, the recent "Nord Stream 2" pipeline project consists of the construction of two parallel inlet and outlet natural gas pipelines through the Baltic Sea (Hirschhausen et al., 2018). In such tandem arrangements, in addition to the usual environmental loads, the horizontal distance between pipelines can also affect the resulting flow and scour patterns. The distance between two long parallel pipelines may change due to on-bottom instability of the pipelines during the interaction between the hydrodynamic loading, the surrounding soil and the pipelines (Gao et al., 2012; Shi et al., 2019). Therefore, it is important to investigate the effect of the distance between two tandem pipelines on scour. Zhao et al. (2015) performed numerical studies involving the local scour around two pipelines in tandem in steady currents. In their work, the numerical model was validated against experiments. Specifically, horizontal gap ratios (defined as the horizontal gap distance separating the two pipelines G divided by their diameter D) ranging from 0.5 to 5 were investigated numerically for current-alone cases. It was found that the scour depth increases with horizontal gap ratios between 0.5 and 2.5, reaching a maximum at $G/D = 2.5$. Zhang et al. (2017) carried out a series of experiments involving scour beneath two tandem pipelines in steady currents with G/D ranging from 0 to 5.9. They found that for horizontal gap ratios between 0 and 3, the equilibrium scour depth beneath the downstream pipeline is slightly larger than that upstream. However, for larger gap ratios between 3 and 5.9, the equilibrium scour depth beneath the downstream pipeline is slightly smaller than that upstream. Their results also showed that the time scale of scour beneath the downstream pipeline is generally larger (by up to a factor 4) than that for the upstream pipeline.

The present work focuses on the numerical investigation of local scour beneath two tandem pipelines subject to wave-plus-current conditions, which has not been previously studied in a detailed manner. A fully-coupled hydrodynamic and morphologic model based on RANS equations coupled with the $k-\omega$ turbulence closure is applied. The same turbulence models have been successfully used in previous scour studies of Fuhrman et al. (2014), Baykal et al. (2015), Larsen et al.

(2016), Bayraktar et al. (2016) and Larsen et al. (2017). The model will be validated against existing experimental measurements involving pure-current induced scour beneath a single pipeline in the live-bed regime (Mao, 1986) as well as against experimentals involving live-bed scour beneath two pipelines in tandem (Zhao et al., 2015). The present model will then be applied to simulate the local scour beneath two tandem pipelines in the wave-plus-current conditions for a variety of *KC* and relative current strengths *m*. Various horizontal gap ratios ranging from $G/D = 1$ to 4 will be considered.

2. Numerical model description

2.1. Hydrodynamic and turbulence models

The present numerical model solves the incompressible unsteady Reynolds-averaged Navier-Stokes (URANS) equations with the $k-\omega$ turbulence model (Wilcox, 2006, 2008) as the closure. The equations governing the flow in the Cartesian coordinate system include a continuity equation and incompressible URANS equations:

$$\frac{\partial u_i}{\partial x_i} = 0 \tag{1}$$

$$\frac{\partial u_i}{\partial t} + u_j\frac{\partial u_i}{\partial x_j} = -\frac{1}{\rho}\frac{\partial p}{\partial x_i} + \frac{\partial}{\partial x_j}\left[2\nu S_{ij} + \frac{\tau_{ij}}{\rho}\right] + F_i \tag{2}$$

where u_i are the mean velocities, x_i are the Cartesian coordinates, $\rho = 1000$ kg/m^3 is the fluid density, p is the pressure, $\nu = 10^{-6}$ m^2/s is the fluid kinematic viscosity, F_i is the external body force used to drive the flow, S_{ij} is the mean-strain-rate tensor defined as

$$S_{ij} = \frac{1}{2}\left(\frac{\partial u_i}{\partial x_j} + \frac{\partial u_j}{\partial x_i}\right) \tag{3}$$

τ_{ij} is the Reynolds stress tensor that defined according to the constitutive relation given by

$$\frac{\tau_{ij}}{\rho} = -\overline{u_i' u_j'} = 2\nu_T S_{ij} - \frac{2}{3}k\delta_{ij} \tag{4}$$

where δ_{ij} is the Kronecker delta, k is the turbulent kinetic energy density expressed as

$$k = \frac{1}{2}\overline{u_i' u_i'} \tag{5}$$

and ν_T is the eddy viscosity. In the present work this is defined by

$$\nu_T = \frac{k}{\tilde{\omega}} \tag{6}$$

where the $\tilde{\omega}$ is defined by

$$\tilde{\omega} = \max\left\{\omega, C_{\lim}\sqrt{\frac{2S_{ij}S_{ij}}{\beta^*}}\right\}, \quad C_{\lim} = \frac{7}{8} \tag{7}$$

The two-equation $k-\omega$ turbulence model is used in the present study as a closure for the URANS equations. The model includes the transport equation of the turbulent kinetic energy k and the specific dissipation rate ω (Wilcox, 2006):

$$\frac{\partial k}{\partial t} + u_j\frac{\partial k}{\partial x_j} = \frac{\tau_{ij}}{\rho}\frac{\partial u_i}{\partial x_j} - \beta^* k\omega + \frac{\partial}{\partial x_j}\left[\left(\nu + \sigma^*\frac{k}{\omega}\right)\frac{\partial k}{\partial x_j}\right] \tag{8}$$

$$\frac{\partial \omega}{\partial t} + u_j\frac{\partial \omega}{\partial x_j} = \alpha\frac{\omega}{k}\frac{\tau_{ij}}{\rho}\frac{\partial u_i}{\partial x_j} - \beta\omega^2 + \frac{\sigma_d}{\omega}\frac{\partial k}{\partial x_j}\frac{\partial \omega}{\partial x_j} + \frac{\partial}{\partial x_j}\left[\left(\nu + \sigma\frac{k}{\omega}\right)\frac{\partial \omega}{\partial x_j}\right] \tag{9}$$

where

$$\sigma_d = H\left\{\frac{\partial k}{\partial x_j}\cdot\frac{\partial \omega}{\partial x_j}\right\}\sigma_{d0} \tag{10}$$

where $H\{\cdot\}$ denotes the Heaveside step function, which takes value 1 if the argument is positive and takes 0 otherwise. The standard closure coefficients are: $\alpha = 0.52$, $\beta = 0.0708$ (constant for two-dimensional problems), $\beta^* = 0.09$, $\sigma = 0.5$, $\sigma^* = 0.6$, $\sigma_{d0} = 0.125$.

In Eqn. (2), the body force F_i is implemented to drive the flow. In the present work, preliminary one-dimensional vertical (1DV) pure flow simulations driven by the body force without morphology are carried out, in order to achieve a fully developed wave-plus-current boundary inlet. The one-dimensional body force of combined waves and current is given by (Larsen et al., 2016):

$$F_1 = U_m\frac{2\pi}{T_w}\cos\left(\frac{2\pi}{T_w}t\right) + \frac{U_{fc}^2}{h} \tag{11}$$

where U_m is the near-bed orbital velocity amplitude of the oscillating flow, T_w is the wave period, U_{fc} is the desired friction velocity of the pure-current, and h is the domain height. After the 1DV flow simulation reaches the equilibrium state, the velocity field, k and ω at the inlet boundary are applied as the boundary inlet for the scour simulations. The body force is then set to zero in the scour simulations as the flow will be driven by the Dirichlet condition at the inlet.

2.2. Sediment transport and morphological models

2.2.1. Bed load transport

The present sediment transport model consists of a bed load transport model and a suspended load transport model. A full description and numerical implementation of the model can be found in Jacobsen (2011) and Jacobsen and Fredsoe (2014). The bed load transport model is based on the work of Roulund et al. (2005) which is a generalized three-dimensional extension of the transport formulation by Engelund and Fredsøe (1976). The bed load sediment transport rate q_B can be written as (Fredsøe and Deigaard, 1992)

$$q_B = \frac{\pi}{6}d^3\frac{p_{EF}}{d^2}U_B \tag{12}$$

where d is the median grain diameter, U_B is the bed load particle moving velocity, for which the detailed derivation can be found in Fredsøe and Deigaard (1992) and Roulund et al. (2005). In the present two-dimensional context, the expression for U_B is given by

$$U_B = aU_f\left(1 - 0.7\sqrt{\frac{\theta_{c0}}{\theta}}\left(cos\left(\gamma\right) - \frac{1}{\mu_d}sin\left(\gamma\right)\right)\right) \tag{13}$$

where $a \approx 10$ is a non-dimensional coefficient and U_f is the friction velocity, such that aU_f denotes the flow velocity at a distance of the order of magnitude d from the bottom (Fredsøe and Deigaard, 1992). γ is the slope angle; p_{EF} is the percentage of particles in motion in the surface layer of the bed, expressed by Engelund and Fredsøe (1976).

$$p_{EF} = \left[1 + \left(\frac{\frac{1}{6}\pi\mu_d}{\theta - \theta_c}\right)^4\right]^{-1/4} \tag{14}$$

where μ_d is the dynamic friction coefficient. In the present work, the value of μ_d is specified as 0.7, following Fuhrman et al. (2014) and Larsen et al. (2016). The Shields parameter θ is defined by

$$\theta = \frac{U_f^2}{(s-1)gd} \tag{15}$$

where $s = \rho_s/\rho$ is the specific gravity of the sediment grains, with ρ_s

being the density of the sediment grains. The critical Shields parameter θ_c for the incipient motion of the particles is taken as (appropriate for two-dimensional problems):

$$\theta_c = \theta_{c0}\left(\cos(\gamma) - \frac{1}{\mu_s}\sin(\gamma)\right) \tag{16}$$

where θ_{c0} is the critical Shields parameter for a horizontal bed and μ_s is the static friction coefficient. In the present study, $\theta_{c0} = 0.045$ and $\mu_s = 0.65$ are utilized, as in Larsen et al. (2016).

2.2.2. Suspended load transport

The suspended load is computed by solving a turbulent-diffusion equation based on the continuity of the concentration (Fredsøe and Deigaard, 1992; Jacobsen, 2011).

$$\frac{\partial c}{\partial t} + (u_j - w_s\delta_{j3})\frac{\partial c}{\partial x_j} = \frac{\partial}{\partial x_j}\left[\left(\nu + \beta_s\frac{k}{\omega}\right)\frac{\partial c}{\partial x_j}\right] \tag{17}$$

where c is the suspended sediment concentration, w_s is the settling velocity, β_s is the factor that is dependent on the grain size and level of turbulence which describes the ratio between sediment particle diffusivity and the eddy viscosity (Rijn, 1984). $\beta_s = 1$ is used in the present study, the same as that in Fuhrman et al. (2014).

A reference concentration c_b is used at the reference level b. In the present work, $b = 3.5d$ is utilized following Fuhrman et al. (2014). For c_b, the formulation proposed by Engelund and Fredsøe (1976) is utilized:

$$c_b = \frac{c_0}{\left(1 + \frac{1}{\lambda_b}\right)^3} \tag{18}$$

where $c_0 = 0.65$ is the maximum value for volumetric concentration, and λ_b is the linear concentration expressed by

$$\lambda_b^2 = \frac{\kappa^2\alpha_1^2}{0.013s\theta}\left(\theta - \theta_c - \frac{\pi}{6}\mu_d p_{EF}\right) \tag{19}$$

The settling velocity w_s is calculated according to Fredsøe and Deigaard (1992):

$$w_s = \sqrt{\frac{4(s-1)gd}{3c_D}} \tag{20}$$

where the drag coefficient is $c_D = 1.4 + 36/R$, and the settling Reynolds number is defined by $R = \frac{w_s d}{\nu}$.

2.2.3. Morphology

The morphological model is based on the sediment continuity (Exner) equation:

$$\frac{\partial h_b}{\partial t} = \frac{1}{1-n}\left[-\frac{\partial q_{Bi}}{\partial x_i} + D_s + E_s\right], i = 1, 2 \tag{21}$$

where h_b is the bed height, n is the porosity which take 0.4 in the present study, D_s is the deposition and E_s is the erosion:

$$D_s = (w_s - v)c_b \tag{22}$$

$$E_s = \left(\nu + \beta_s\frac{k}{\omega}\right)\left.\frac{\partial c}{\partial x_3}\right|_{x_3 = b} \tag{23}$$

In the present simulations, the morphological time step is the same as the hydrodynamic time step i.e. no morphological acceleration of any kind is utilized. To prevent the excess steepness of the bed, the sand slide model of Niemann et al. (2010) in two-dimensional is incorporated in the present study with the angle of repose of 32°. The sand slide model uses a geometrical approach (Marieu et al., 2008; Niemann et al., 2010) to prevent the un-physical steepening of the scour shape. The implementation of the sand slide model is described in Jacobsen (2011).

2.3. Boundary conditions

The hydrodynamic boundary conditions are specified as follows.

- At the seabed and pipeline surfaces, no-slip boundary conditions are used, i.e., the velocities at the walls are zero. The seabed is modelled as a hydraulically rough wall where the friction velocity U_f is determined by the tangential velocity at the nearest cell center based on an assumed logarithmic velocity distribution, as described in Fuhrman et al. (2014). The pipeline surface is modelled as a hydraulically smooth wall where the friction velocity U_f is determined based on the profile proposed by Cebeci and Chang (1978). The generalized wall functions for k and ω are presented in Fuhrman et al. (2014).
- At the top boundary, a frictionless lid is modelled at which the vertical velocity is zero and the horizontal velocities and other hydrodynamic quantities have zero normal gradients.
- At the inlet boundary, a Dirichlet boundary is specified with time-varying u, k and ω, taken from the preliminary 1DV simulations. The outlet boundary is specified by a Neumann condition with zero normal velocity gradient and zero pressure.

For the sediment transport model, the boundary conditions for the suspended sediment concentration c is specified as follows.

- At the top and pipeline boundaries, a zero-flux condition for c is specified.
- At the bottom seabed boundary, a reference concentration is specified, as presented in Eqn. (18). The reference concentration is not imposed at the bottom wall but is at a reference distance of $3.5d$ from the seabed.
- At the inlet and outlet boundaries, c is specified with a zero normal gradient.

3. Model validation

The present numerical model has been validated in Fuhrman et al. (2014) and Larsen et al. (2016). Fuhrman et al. (2014) validated the present model for scour around a pipeline in waves against the measurement of Sumer and Fredsøe (1990). Larsen et al. (2016) validated the present model for scour around a pipeline in the current against Mao (1986) and in the wave-plus-current condition against the experimental findings of Sumer and Fredsøe (1996). The present work uses the same model but with new mesh for the single pipeline case. Therefore, additional validations are conducted in the present study.

The computational meshes in the present study for a single pipeline and two pipelines in tandem are shown in Fig. 1 (sub-plots (a) and (b), respectively). A small initial scour hole $S_0/D = 0.15$ is needed to ensure that there are cells beneath the pipeline. First, the computational mesh setup for a single pipeline will be validated by reproducing the live-bed scour experiment of Mao (1986). The time series of the non-dimensional scour depth S/D development and the scour profiles at two time instants will be compared to the experimental data in section 3.1. Then, the computational mesh for a single pipeline is extended for two pipelines in tandem, as shown in Fig. 1a. For this purpose, the present model will be validated against the experiments of Zhao et al. (2015), involving live-bed scour around two tandem pipelines in a current. The bed profiles at the corresponding time instants will be compared in section 3.2. In all the cases, the smallest cells near the pipeline have a height of $0.003D$ and the smallest cells near the seabed have a height of $0.5d$.

3.1. Validation against the experiment of scour beneath a single pipeline

In this section the live-bed scour experiment in Mao (1986) is reproduced using the present model and mesh. The Shields parameter θ

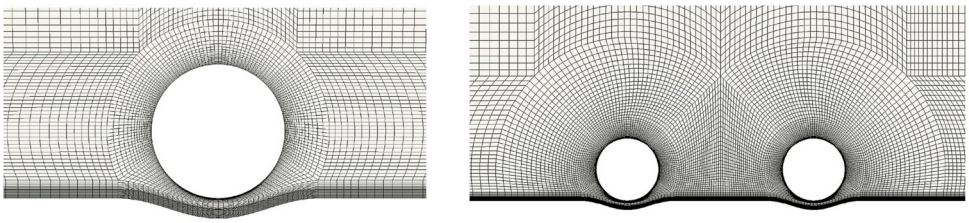

(a) Mesh around a single pipeline. (b) Mesh for two pipelines in tandem.

Fig. 1. Mesh setup.

is 0.098 for both the experiment and the present simulation. The pipeline diameter and the grain size in Mao (1986) is $D = 0.1$ m and $d = 0.36$ mm. In the present simulation, $D = 0.03$ m and $d = 0.19$ mm. Following the arguments of Larsen et al. (2016), this is justifiable as non-dimensional comparison between the present numerical simulation and the experiment of Mao (1986) are performed in terms of S/D over the non-dimensional time t^* which is expressed as

$$t^* = \frac{\sqrt{g(s-1)d^3}}{D^2} t \tag{24}$$

where t is the physical time. It is ensured that the non-dimensional scour developments are comparable between two different scales once the Shields parameter is kept the same. The friction velocity U_f is calculated using Eqn. (15) and is equal to 0.017 m/s in the present simulation. The specific gravity of the sediment grains is $s = 2.65$ for both the experiment (Mao, 1986) and the present simulation. An initial hole of $S_0/D = 0.15$ is specified in the numerical simulation. Therefore, an approximation time that is used to develop the initial hole is added to compare the numerical time series to the corresponding experimental results of Mao (1986). The approximation time is calculated by $t_0 = \frac{S_0/D}{dS/dt}$. dS/dt is the initial scour rate calculated by the scour depth growth between the initial two saved time instants divided by the saved time step. For the present validation case, the simulation results are saved every 3 s, corresponding to $\Delta t^* = 0.035$. The non-dimensional scour depths S/D over the non-dimensional time t^* from the present numerical simulation and the experiment of Mao (1986) are compared in Fig. 2a. It is shown in Fig. 2a that the present numerical results are in good agreement with the experimental measurement by Mao (1986). The final equilibrium scour depth reaches around $0.7D$ for both the numerical simulation and the experiment. As mentioned before, the expected equilibrium scour depth should be approximately constant (Sumer and Fredsøe, 1990) as $\frac{S_e}{D} = 0.6 \pm 0.2$. Fig. 2a compares the profiles between the numerical prediction and the experimental measurement. It shows that the predicted downstream shoulder is slightly smaller than the experiment at the first time instant ($t^* = 0.24$) and slightly larger than the experiment at the second time instant ($t^* = 4.86$). The predicted profiles are generally consistent with the experimental measurement and the scour depths beneath the pipeline are highly matched. Therefore, the present computational mesh setup and grid resolution for a single pipeline have been validated.

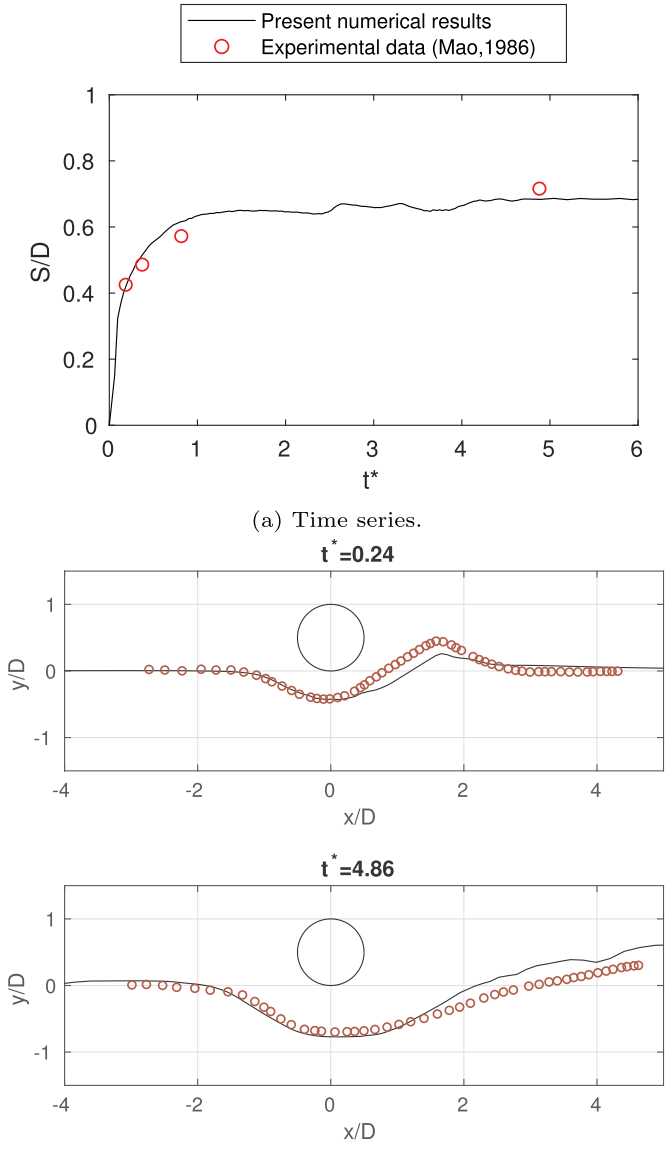

(a) Time series.

(b) Scour profiles.

Fig. 2. Comparison of the present numerical results of scour depth development to the experimental data of Mao (1986), with $\theta = 0.098$ for both the experiment and the present simulation.

3.2. *Validation against the experiment of scour beneath two pipeline in tandem*

To further validate the present model, the experiments conducted by Zhao et al. (2015) will be considered, involving scour around two pipelines in a steady current. In Zhao et al. (2015), two laboratory tests were conducted with two identical pipelines having $D = 0.15$ m, having two different horizontal gap ratios $G/D = 0.5$ and 3. The sediment that was used in the model test has a median diameter d of 0.24 mm and a specific gravity of $s = 2.65$. The incoming steady flow velocity is 0.65 m/s at a height of 0.15m above the sand bed surface, which corresponds to $U_f = 0.029$ m/s and $\theta = 0.218$.

The present study first conducted the 1DV simulation to ensure that the incoming flow at the inlet reaches its equilibrium state. Then the scour simulations are conducted for both the $G/D = 0.5$ and $G/D = 3$ cases. The bed profiles computed from the numerical simulations at different time instants are compared with the experimental data reported by Zhao et al. (2015) in Fig. 3. It shows that the bed profiles

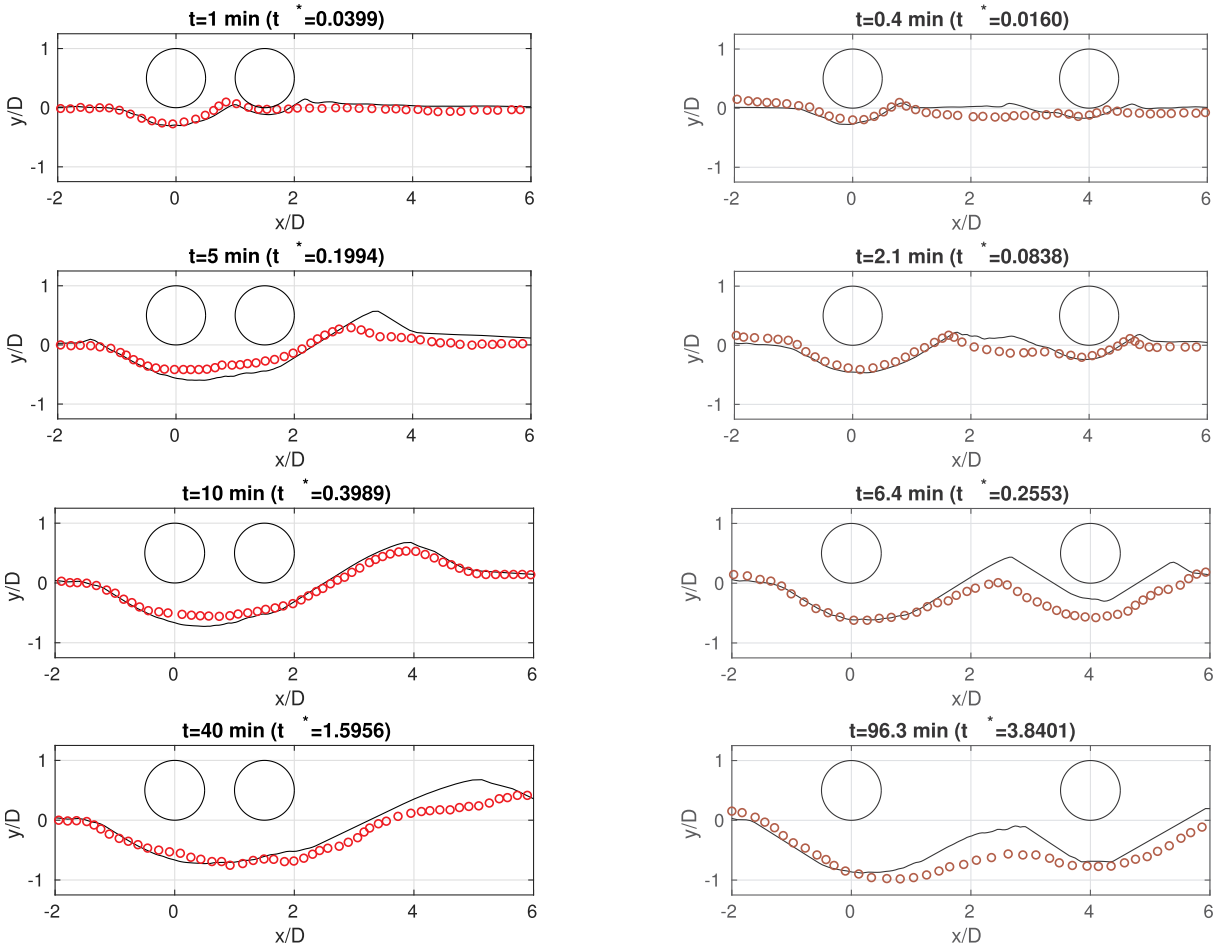

(a) Horizontal gap ratio $G/D = 0.5$. (b) Horizontal gap ratio $G/D = 3$.

Fig. 3. Comparison of the bed profiles between the present numerical simulations and the experimental measurement of Zhao et al. (2015). Left column: $G/D = 0.5$; Right column: $G/D = 3$.

solved by the present numerical model are in a reasonable agreement with Zhao et al. (2015)'s experimental measurements. For the $G/D = 0.5$ case, the maximum scour depth is located in between the two pipelines. No ripples are observed between two pipelines after the test time of 5 min. For the $G/D = 3$ case, the numerical result of scour depth beneath the downstream pipeline is slightly smaller than the experimental data by Zhao et al. (2015) at $t = 6.4$ min. At $t = 96.3$ min, the berm in between the two pipelines from the numerical simulation is more obvious than that from the experiment. However, the final scour depths below the centers of two pipelines are generally in good agreement with the experimental data. Therefore, the present numerical model for predicting scour beneath two pipelines in tandem and the present grid resolution for two pipelines have been validated.

4. Model application

A sketch of the present numerical model of scour beneath two pipelines in tandem is shown in Fig. 4. The pipelines are placed on the seabed with the upstream pipeline's bottom at the origin (x, y) = (0, 0). The horizontal gap ratio, i.e., the horizontal gap distance between the two pipelines over the pipeline diameter G/D takes the values of 1, 2, 3 and 4 in the present study. An initial hole with a depth of $S_0/D = 0.15$ is set for both pipelines. In the present simulations, the pipeline diameter is $D = 0.03$ m and the grain size is $d = 0.19$ mm. The specific gravity of the sediment grains is $s = 2.65$.

The wave-plus-current conditions simulated in the present work are given in Table 1, with six different KC ranging from 5.6 to 30, combined

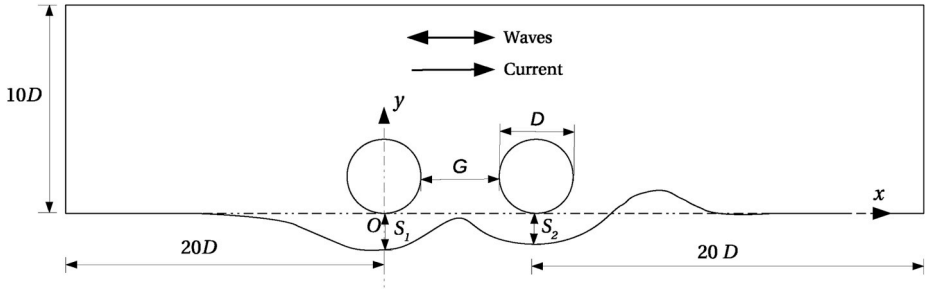

Fig. 4. A sketch of the numerical layout for scour beneath two pipelines in tandem.

Table 1
Wave-plus-current conditions in the present study. Each *KC* and its corresponding T_w and U_m are taken from the references. The present study simulates wave-plus-current conditions by adding different levels of U_c to the pure-wave conditions. U_c is calculated while the relative current strength m is 0, 0.25 and 0.5.

KC	Reference	T_w (s)	U_m (m/s)	U_c (m/s)			θ_{cw}		
				m = 0	m = 0.25	m = 0.5	m = 0	m = 0.25	m = 0.5
5.6	Fredsøe et al. (1991)	1.1	0.153	0	0.051	0.153	0.119	0.125	0.161
11	Sumer and Fredsøe (1990)	1.22	0.24	0	0.080	0.240	0.177	0.191	0.269
15	Sumer and Fredsøe (1990)	2.5	0.177	0	0.059	0.177	0.091	0.099	0.141
19.6	Fredsøe et al. (1991)	3	0.196	0	0.065	0.196	0.092	0.102	0.150
25.3	Fredsøe et al. (1991)	3.51	0.216	0	0.072	0.216	0.094	0.105	0.161
30	Fuhrman et al. (2014)	3.5	0.257	0	0.086	0.257	0.120	0.136	0.212

with three different current strengths for each *KC*. In Table 1, U_c is calculated while the relative current strength m is 0, 0.25 and 0.5, with m defined by

$$m = \frac{U_c}{U_c + U_m} \tag{25}$$

where U_m is the near-bed orbital velocity amplitude of the oscillating flow and U_c is the current velocity at the center of the pipeline. With this definition $m = 0$ corresponds to a pure-wave condition and $m = 1$ corresponds to a pure-current condition.

According to Sumer and Fredsøe (1996), when $m > 0.7$, (and similarly according to Larsen et al. (2016), when $m \geq 0.5$), the current effect is dominant, and the scour depths are very similar to those in the pure-current conditions. The pure-current ($m = 1$) induced scour beneath two tandem pipelines has been numerically simulated by Zhao et al. (2015) and experimentally investigated by Zhang et al. (2017). Therefore, the present work focuses on the range of $m = 0$ to 0.5, i.e., from pure-wave conditions ($m = 0$) to an essentially equal strength of the wave and current (corresponding to $m = 0.5$). Fig. 5 shows the time series of free stream velocity at the pipeline center with $m = 0$, 0.25 and 0.5, for cases having $KC = 19.6$, as an example.

The far-field Shields parameter θ_{cw} for the wave-plus-current flow is calculated as follows (Soulsby, 1995; Fuhrman et al., 2013; Larsen et al., 2016).

$$\theta_{cw} = \theta_w + \theta_m \tag{26}$$

where θ_w is the is the maximum Shields parameter of the oscillating flow. The maximum near-bed friction velocity induced by the oscillating flow is calculated by

$$U_{fw} = \sqrt{0.5 f_w} U_m \tag{27}$$

Here, following e.g. Larsen et al. (2016), f_w is calculated by taking the maximum among the laminar, smooth-turbulent, and rough-turbulent wave friction factors: $f_w^{lam} f_w^{smooth} f_w^{rough}$.

$$\begin{cases} f_w^{lam} = \dfrac{2}{\sqrt{Re}} \\ f_w^{smooth} = 0.035 Re^{-0.16} \\ f_w^{rough} = \exp\left(5.5\left(\dfrac{a}{k_s}\right)^{-0.16} - 6.7\right) \end{cases} \tag{28}$$

where $Re = U_m \lambda / \nu$ is the Reynolds number, $\lambda = U_m T_w/(2\pi)$ is the characteristic amplitude of free stream orbital motion, the f_w^{smooth} expression is from Fredsøe and Deigaard (1992), and the f_w^{rough} expression is from Fuhrman et al. (2013). The mean Shields parameter θ_m is calculated by

$$\theta_m = \theta_{cur}\left(1 + 1.2\left(\frac{\theta_w}{\theta_{cur} + \theta_w}\right)^{3.2}\right) \tag{29}$$

where θ_{cur} is the Shields parameter calculated from the pure current friction velocity U_{fc}. Table 1 shows that the far-field Shields parameters θ_{cw} of the present wave-plus-current cases are all larger than the critical Shields parameter $\theta_{c0} = 0.045$. Therefore, the present cases in wave-plus-current conditions are all in the live-bed regime. For all the simulated cases, a warm-up period (with morphology turned off) of $t = 10T_w$ is applied.

5. Results and discussion

The discussion of the results will start from presenting the scour profile evolution and time series of scour depth development for representative cases with $m = 0$, $m = 0.25$ and $m = 0.5$, respectively. Then the equilibrium depths of all the cases will be summarized and discussed.

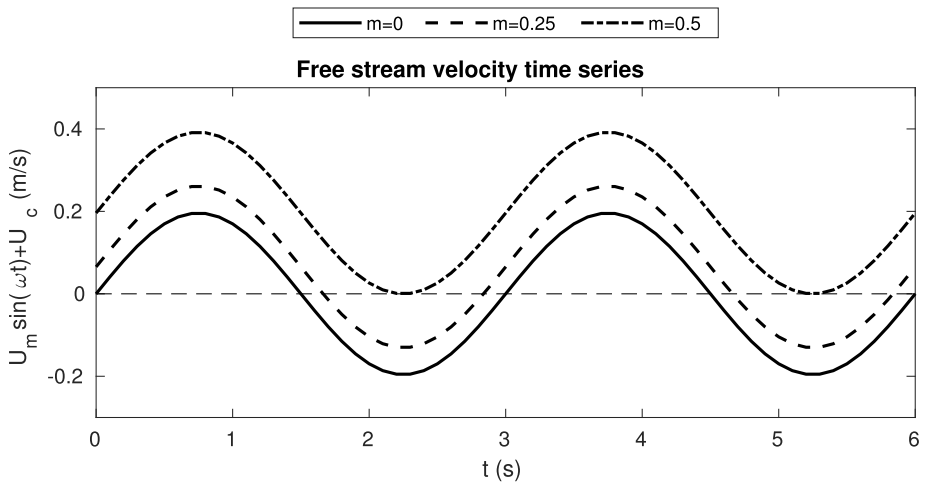

Fig. 5. Free stream velocity of wave-plus-current in a time series.

5.1. Profile evolution and time series

5.1.1. Pure-wave conditions $m = 0$

When $m = 0$, i.e. pure-wave conditions, the scour profile in the vicinity of the upstream and the downstream pipelines is generally symmetric. Fig. 6 shows the scour profiles in a pure-wave condition with $KC = 30$. It is seen that a small berm emerges between two pipelines at the initial time. For each G/D, the berm in between two pipelines is gradually eroded over time and becomes less visible than that at the beginning. When the horizontal gap ratio is larger, the berm is more visible during the equilibrium stage. It is also noted that the maximum scour depths of the final scour profile are not located right below the center of the pipelines. The maximum scour depths gradually move towards the middle of the two pipelines during the development.

The time-averaged scour depth development with $m = 0$, $KC = 30$ can be seen in the left column of Fig. 7, which depicts time series of the scour beneath two pipelines in tandem for varying horizontal gap ratios. It is shown that the time-averaged scour depths beneath the upstream and the downstream pipelines are generally symmetric.

It is noted that the number of the berms that are formed in between the tandem pipelines is influenced by both G/D and KC. As KC is proportional to the ratio of the amplitude of free stream orbital motion to the pipeline diameter, it is expected that for large horizontal gap ratios, more berms in between the two pipelines can be formed for a small KC. Fig. 8 presents computed scour profiles with different KC during the equilibrium stage with large horizontal gap ratio, i.e. $G/D = 4$. It is seen that for $KC = 5.6$, three berms are formed between two pipelines at the equilibrium stage. For $KC = 15$, two berms are formed in between two pipelines. As KC increases to over 15, only one berm is observed between the tandem pipelines, as shown in Fig. 8 e.g. with $KC = 25.3$. It should be mentioned that the asymmetric form of the berms in $KC = 15$ is a momentary phenomenon, since the profile still changes cyclically during the equilibrium stage. The number of berms that are formed between the pipelines can be related to the natural length of vortex ripples. Following Brøker (1985) and Fuhrman et al. (2014), the nature length of the vortex ripples is calculated by $\lambda_r/D = 1.2/(2\pi)\cdot KC$. For $KC = 5.6$, λ_r/D is calculated as 1.07, meaning that we can expect three vortex ripples between the pipelines at $G/D = 4$. For $KC = 15$, λ_r/D is calculated as 2.86, so there is maximum two vortex ripples between the pipelines with $G/D = 4$. For $KC = 25.3$, λ_r/D is 4.83 so that only one vortex ripple can be formed between the pipelines with $G/D = 4$.

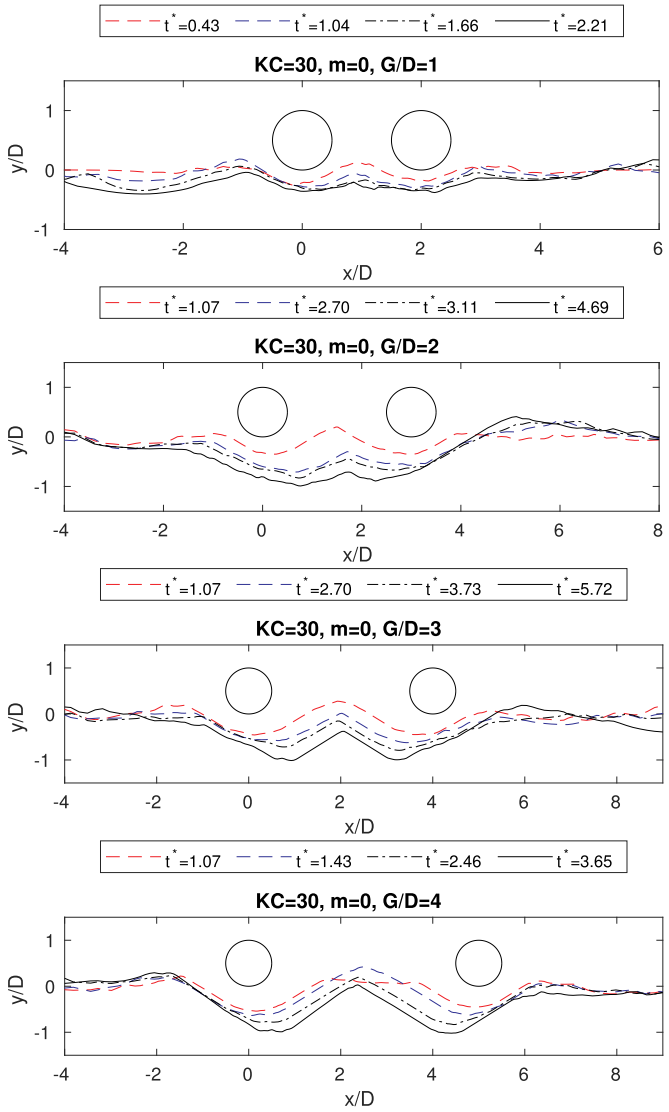

Fig. 6. Scour profiles for $m = 0$, pure-wave condition with $KC = 30$.

5.1.2. Waves with weak current $m = 0.25$

We will now consider waves with a relatively weak current, corresponding specifically to the flows with $m = 0.25$. Fig. 9 presents a comparison of the scour profiles between the $m = 0$ and $m = 0.25$ cases with $KC = 15, G/D = 2$; $KC = 25.3, G/D = 2$ and $KC = 25.3, G/D = 4$. It is shown that with $m = 0.25$, the scour profiles resemble those under pure-wave conditions, but with slightly less symmetry. Especially, in Fig. 9c with $KC = 25.3, m = 0.25, G/D = 4$, the asymmetry of the scour profile is more apparent than those with $m = 0.25$ in Fig. 9a and b. Fig. 9 demonstrates that for these three cases the shoulders at the downstream are more eroded with $m = 0.25$ compared to $m = 0$. Fig. 9a and b present the scour profiles with the same G/D but different KC. It is seen that the scour profile patterns (with $m = 0$ and 0.25, respectively) are similar with different KC. With a larger KC, the scour depth increases for both $m = 0$ and 0.25. Fig. 9b and c present the scour profiles with the same KC but different G/Ds. It is shown that the scour depth also increases when G/D increases from 2 to 4 for both $m = 0$ and 0.25.

The scour time series with $m = 0.25$ are also compared with those with $m = 0$ in Figs. 7 and 10, respectively. It is generally observed that with $m = 0.25$, the scour depths at the equilibrium stage does not differ much from those with $m = 0$. The result is consistent with the findings in Larsen et al. (2016), who simulated the wave-plus-current induced scour beneath a single pipeline. They found that a low value of m leads to scour pattern quite close to pure-wave cases. It is seen that for the $G/D = 1$ cases, the scour time series with $m = 0.25$ are very close to those with $m = 0$, since the lee-wake vortex shedding is largely suppressed in between the two pipelines. However, it appears that when the horizontal gap ratio increases, the two pipelines eventually have different scour depths under the asymmetric effect of wave-plus-current conditions, although the difference is minor, as seen in Figs. 7 and 10 at $G/D = 2$, 3, and 4. Here, the downstream pipeline has a slightly larger scour depth than the upstream pipeline after reaching equilibrium.

5.1.3. Waves with strong current $m = 0.5$

We will now consider waves with a strong current, corresponding specifically to the flows with $m = 0.5$. As shown before in Fig. 5, when $m = 0.5$, the undisturbed free stream velocity is ≥ 0 at all times. This means that the undisturbed free stream flow behaves more like a unidirectional current flow with a fluctuating velocity from 0 to $2U_m$. Therefore, it is expected that with $m = 0.5$ the effect of the current should become more dominant compared to the effect of waves.

Fig. 11 presents the scour profile evolution and the time series with $m = 0.5$, $G/D = 1$ for the case having $KC = 19.6$ as an example. It is seen in Fig. 11a that the scour holes beneath the two tandem pipelines are merged into one large scour hole while reaching equilibrium. This profile shape is similar to that in the validation case involving a steady current, as shown in Fig. 3a. The same phenomenon is observed for $m =$

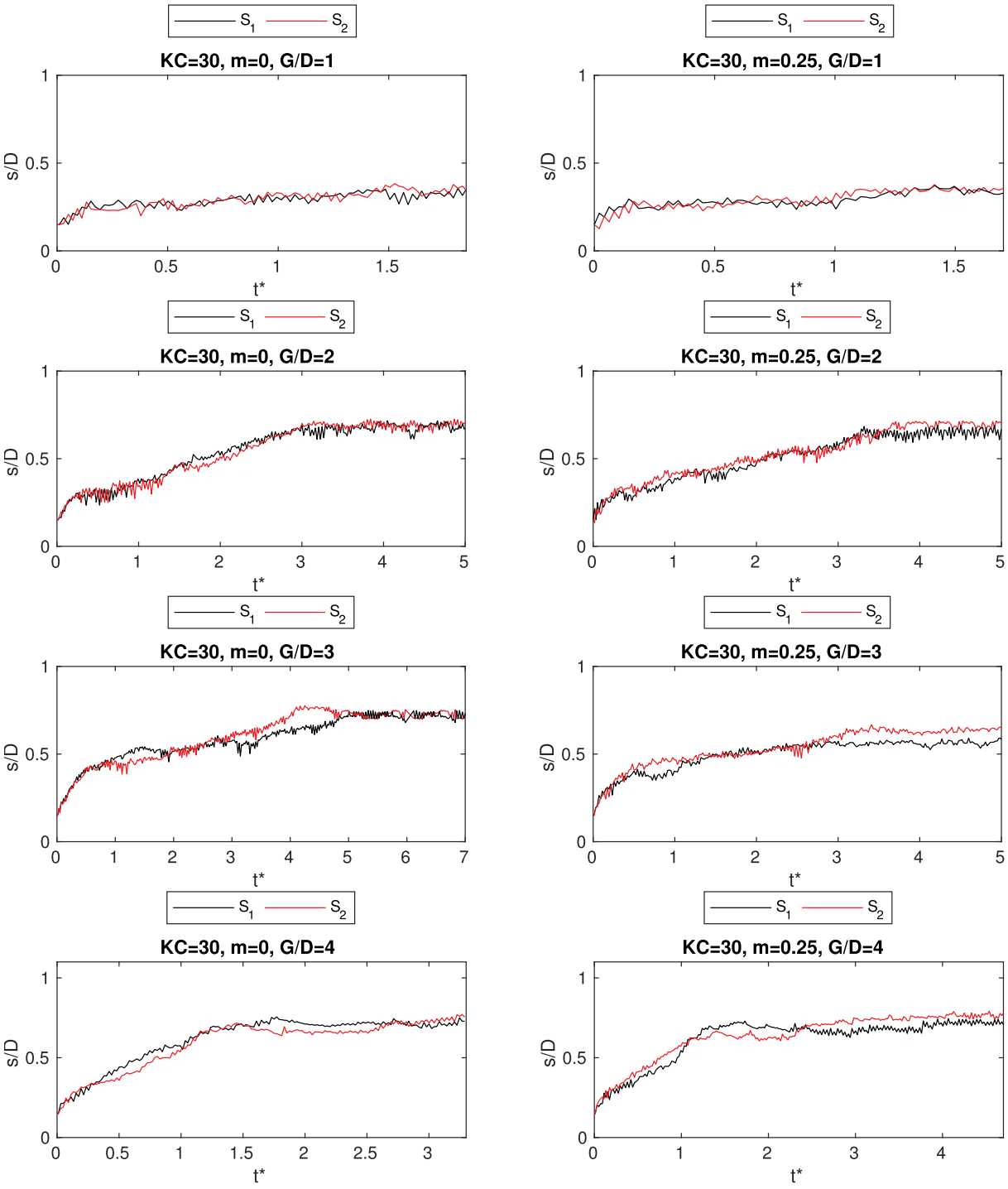

Figure 7. Time series of the scour depths beneath the upstream pipeline (S_1) and the downstream pipeline (S_2) with $KC = 30$. Left column: $m = 0$; Right column: $m = 0.25$.

0.5, $G/D = 1$ cases having all the KC except for $KC = 5.6$. Zhou and Yiu (2006) and Sumner (2010) investigated the flow around two pipelines in the pure current. They found that for $G/D \leq 1$, the two pipelines behave effectively as a single extended body so that the one large scour hole is formed beneath the two tandem pipelines while reaching equilibrium.

It is noticed in Fig. 11 that the development of the scour profile with $m = 0.5$, $G/D = 1$ generally follows a four-stage pattern, as shown in Fig. 11a. At the initial stage, the scour depths beneath the two pipelines are both increased. A berm is formed in between the two pipelines (e.g. $t^* = 0.09$ in Fig. 11a, stage (1) in Fig. 11b). Then, at the second stage, the berm migrates towards the downstream pipeline and the scour hole beneath the downstream pipeline is slightly buried by the sediments transported from upstream. The scour depth beneath the downstream pipeline slightly decreases at this stage (e.g. $t^* = 0.33$ in Fig. 11a, stage (2) in Fig. 11b). The reduction of the scour hole beneath the downstream pipeline at the second stage is explained in Fig. 12 which shows the velocity field and the suspended sediment concentration at a time instant during this stage. As shown in Fig. 12a, the berm in the gap causes flow separation at its lee-side. The main flow is transported along the stoss-side of the berm towards the upper side of the downstream pipeline. Only a small part of the flow pass through the tunnel beneath the downstream pipeline. Due to the low flow velocity and low shear

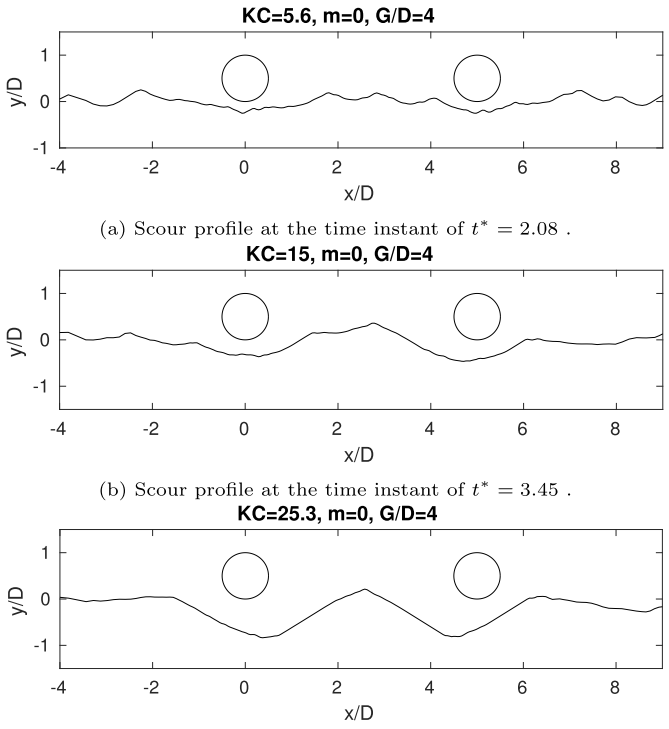

(a) Scour profile at the time instant of $t^* = 2.08$.

(b) Scour profile at the time instant of $t^* = 3.45$.

(c) Scour profile at the time instant of $t^* = 4.85$.

Fig. 8. The number of berms formed in between two pipelines varies with KC at $G/D = 4$.

stress in the downstream tunnel, the small amount of sediments transported from the upstream are mainly trapped inside the tunnel while very little can be transported out. It is noted that for the present cases, both bed load transport and suspended sediment transport play important roles during the scour process. Fig. 12b shows the distribution of the suspended sediment concentration at the second stage. High suspended sediment concentration is observed at the lee-side of the berm. Suspended sediments are transported into the downstream tunnel. At the lee-side of the downstream pipeline, the suspended sediment concentration is relatively low, indicating that very few suspended sediments are transported out of the downstream tunnel, causing a decrease of the scour depth beneath the downstream pipeline. As the berm gradually migrates downstream until it comes to the vicinity of the downstream pipeline, the small gap between the downstream pipeline and the seabed triggers accelerated flow velocity and increased bed shear stress beneath the downstream pipeline. Therefore, the sediments beneath the downstream pipeline are transported out of the downstream scour hole. The height of the berm between the two pipelines is gradually decreased as the sediments formed the berm are washed downstream to the tandem pipelines.

At the third stage, the scour depths beneath the upstream and downstream pipelines are both increasing (e.g. $t^* = 2.77$ in Fig. 11a, stage (3) in Fig. 11b). Fig. 13 shows the velocity field and the suspended load concentration at this stage. With the disappearance of the berm in the gap, the main flow is passing beneath the downstream pipeline, causing high velocity and shear stress at the downstream slope. The depth and width beneath the downstream pipeline are gradually increasing. At this stage, the scour depth beneath the upstream pipeline reaches equilibrium first, while the scour depth beneath the downstream pipeline is still under development. The sediments are transported to the downstream of both pipelines because of the vortex shedding behind the downstream pipeline. At the final stage, the scour profile reaches equilibrium with minor cyclic fluctuations (e.g. $t^* = 5.89$ in Fig. 11a, stage (4) in Fig. 11b). The time series and the corresponding four stages of the scour development with $KC = 19.6, m = 0.5, G/D = 1$ are shown in Fig. 11b. The same phenomenon is seen at other KC except for $KC = 5.6$.

The final scour profile for $KC = 5.6, m = 0.5, G/D = 1$ is shown in Fig. 14. It is seen that the berm in between the two pipelines is not eroded due to the small stroke of the wave motion. Also, for such a low KC, the T_w is also small so that the flow direction changes frequently with a small stroke of wave motion. Therefore, the scour depth does not develop much.

As the horizontal gap distance increases, two pipelines become more independent. Separate scour holes are formed beneath the two pipelines. Therefore, the berm in between the two pipelines will not disappear

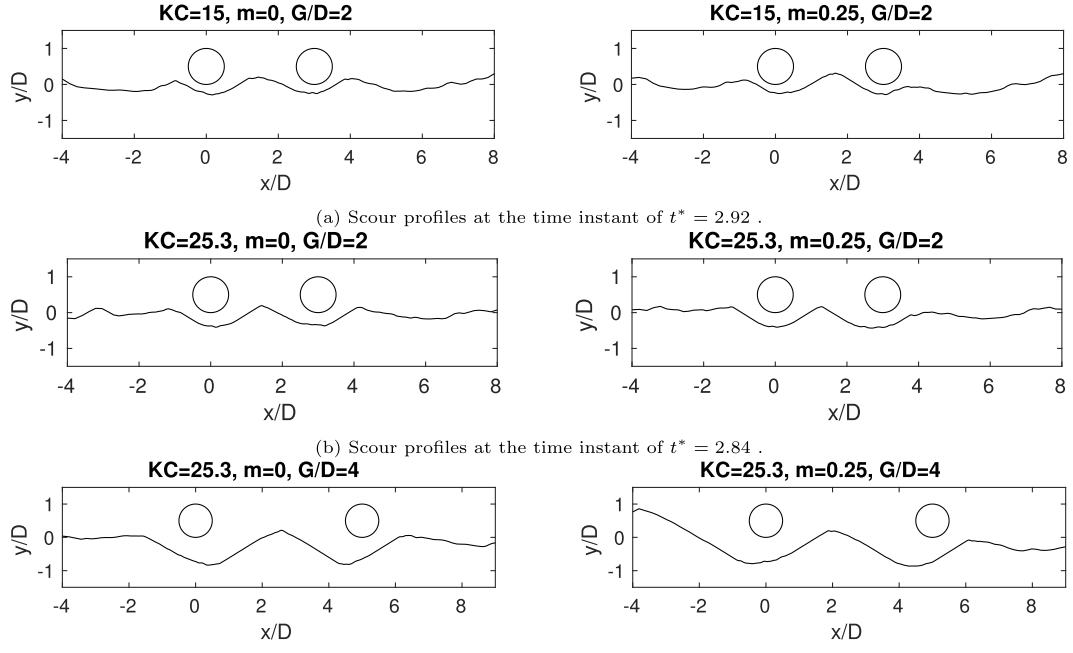

(a) Scour profiles at the time instant of $t^* = 2.92$.

(b) Scour profiles at the time instant of $t^* = 2.84$.

(c) Scour profiles at the time instant of $t^* = 4.85$.

Fig. 9. A comparison of scour profiles during equilibrium stage between $m = 0$ and $m = 0.25$. Left column: $m = 0$; Right column: $m = 0.25$.

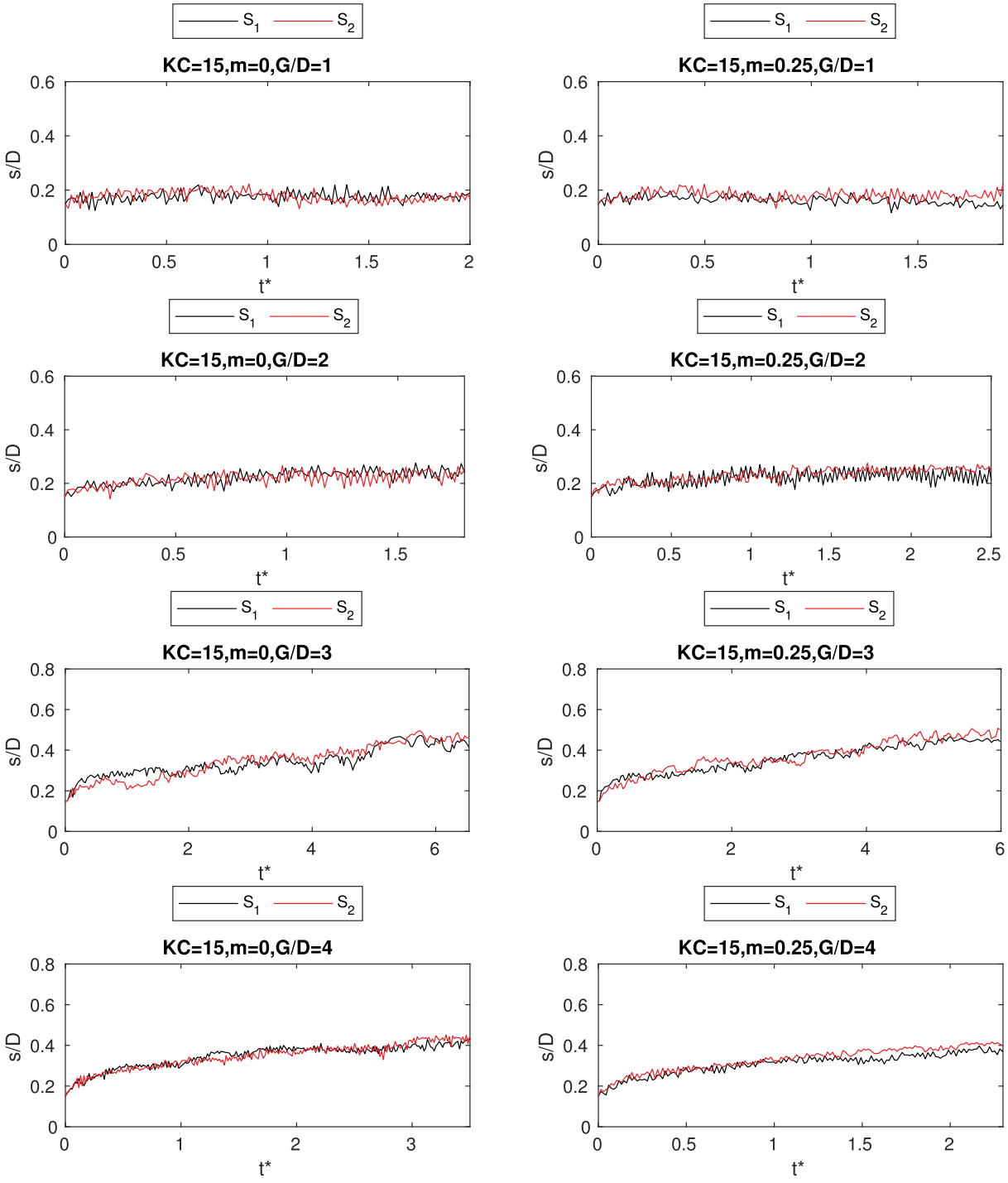

Fig. 10. Time series of the scour depths beneath the upstream pipeline (S_1) and the downstream pipeline (S_2) with $KC = 15$. Left column: $m = 0$; Right column: $m = 0.25$.

even at the equilibrium stage. As shown in Fig. 15 and Fig. 16 (for $m = 0.5$ cases with $KC = 19.6$ and $KC = 25.3$, respectively), at the equilibrium stage, the berm is still present and is located close to the downstream pipelines. It is seen in Fig. 15 that as the horizontal gap distance increases from 2 to 4, the berm height becomes higher after reaching equilibrium. It is also seen that the width of the scour hole beneath the upstream pipeline becomes larger as the horizontal gap distance increases.

Fig. 17 and Fig. 18 present the scour time series with $KC = 11, m = 0.5$ and $KC = 30, m = 0.5$ at $G/D = 1$, 2, 3, and 4. It is observed that the time duration for the scour beneath the downstream pipeline to reach equilibrium is larger than that required for the upstream pipeline. It shows that with $G/D = 1$ the downstream pipeline experiences a greater delay of scour development compared to those with larger horizontal gap ratios. The same as the time series of $KC = 19.6, m = 0.5, G/D = 1$ in Fig. 11b, it is also shown in Figs. 17 and 18 that for $m = 0.5, G/D = 1$ at different KC, the downstream pipeline experiences an initial increase of the scour depth (stage(1)) and then a decrease of the scour depth (stage (2)) during the scour development process.

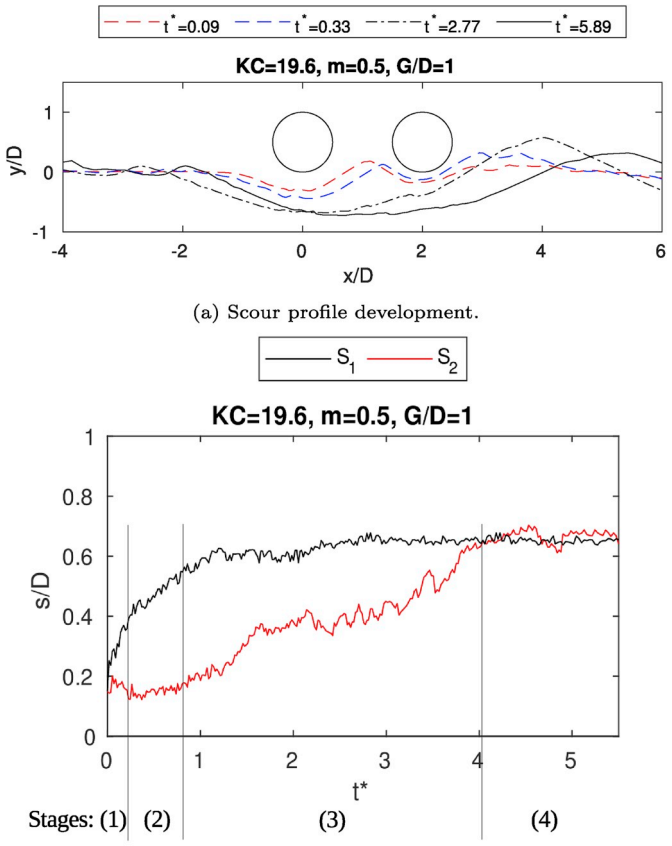

(a) Scour profile development.

(b) Time series.

Fig. 11. Scour profile development and time series of case $KC = 19.6$, $m = 0.5$, $G/D = 1$.

5.2. Equilibrium depths

For all the cases, the equilibrium scour depths beneath the centers of the upstream and downstream pipelines are shown in Figs. 19–21. For $m = 0$ (a pure-wave condition), the time-averaged scour depth development is symmetric below two pipelines. Therefore, only one S_e is shown in Fig. 19. Due to minor fluctuations of the scour depth at the equilibrium stage, S_e is calculated from $(\overline{S_1} + \overline{S_2})/2$, where $\overline{S_1}$ and $\overline{S_2}$ are the average scour depths beneath the upstream and the downstream pipelines over ten wave periods after reaching equilibrium. For a single pipeline in pure-wave conditions, the equilibrium scour depth is a function of the KC number (Sumer and Fredsøe, 1990), $S_e/D = f\{KC\}$, as expressed by the solid line in Fig. 19.

Figs. 20 and 21 present the equilibrium scour depths in combined waves and current with $m = 0.25$ and $m = 0.5$, where the reference lines in the figures correspond to the empirical expressions for the equilibrium scour depth for a single pipeline in combined waves and current given by Sumer and Fredsøe (1996):

$$S_e = S_c F \tag{30}$$

where S_c is the equilibrium scour depth in the pure current ($S_c/D = 0.6 \pm 0.2$). F is calculated by

$$F = \begin{cases} \frac{5}{3}(KC)^{a_m}\exp(2.3b_m), & 0 \le m \le 0.7 \\ 1, & m \ge 0.7 \end{cases} \tag{31}$$

where

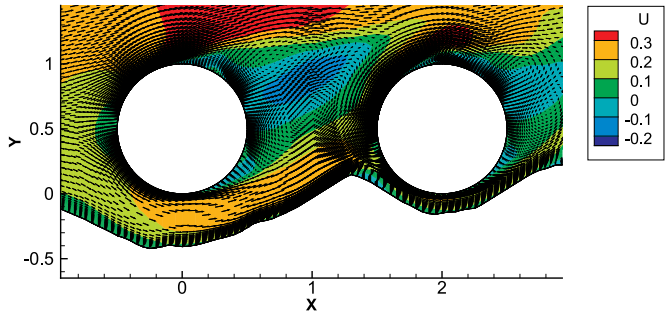

(a) Velocity field (m/s).

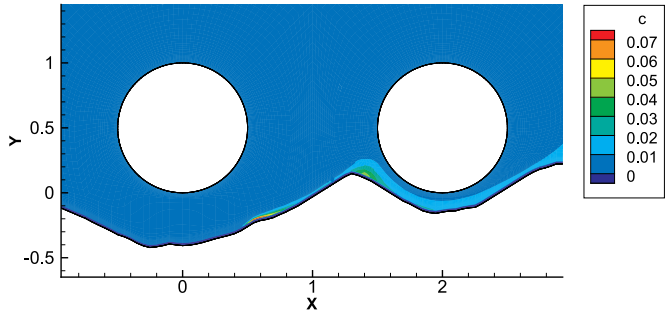

(b) Suspended sediment concentration.

Fig. 12. Velocity field (unit: m/s) and suspended sediment concentration for case $KC = 19.6$, $m = 0.5$, $G/D = 1$. The time instant is $t^* = 0.26$, when the downstream pipeline experiences a decrease of the scour depth (corresponding to stage (2) in Fig. 11b).

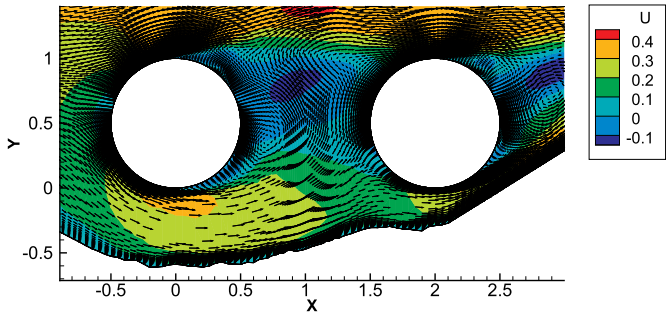

(a) Velocity field (m/s).

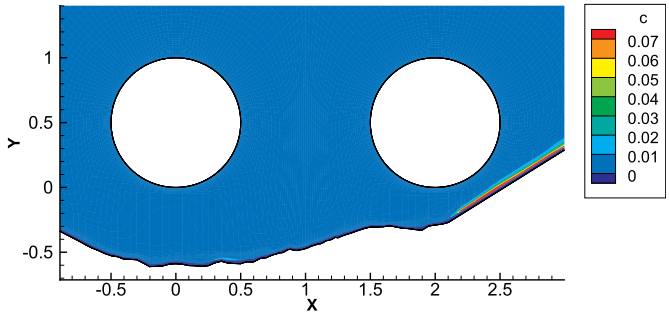

(b) Suspended sediment concentration.

Fig. 13. Velocity field (unit: m/s) and suspended sediment concentration for case $KC = 19.6$, $m = 0.5$, $G/D = 1$. The time instant is $t^* = 1.52$, when the downstream pipeline experiences an increase of the scour depth (corresponding to stage (3) in Fig. 11b).

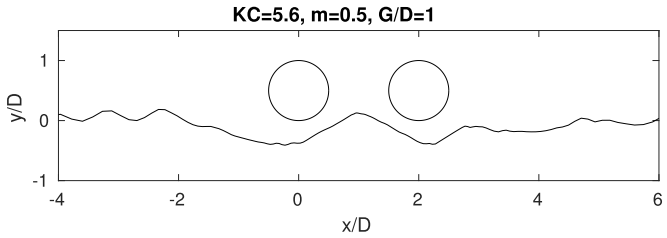

Fig. 14. Scour profile at the equilibrium stage with $KC = 5.6$, $m = 0.5$, $G/D = 1$ at $t^* = 3.29$.

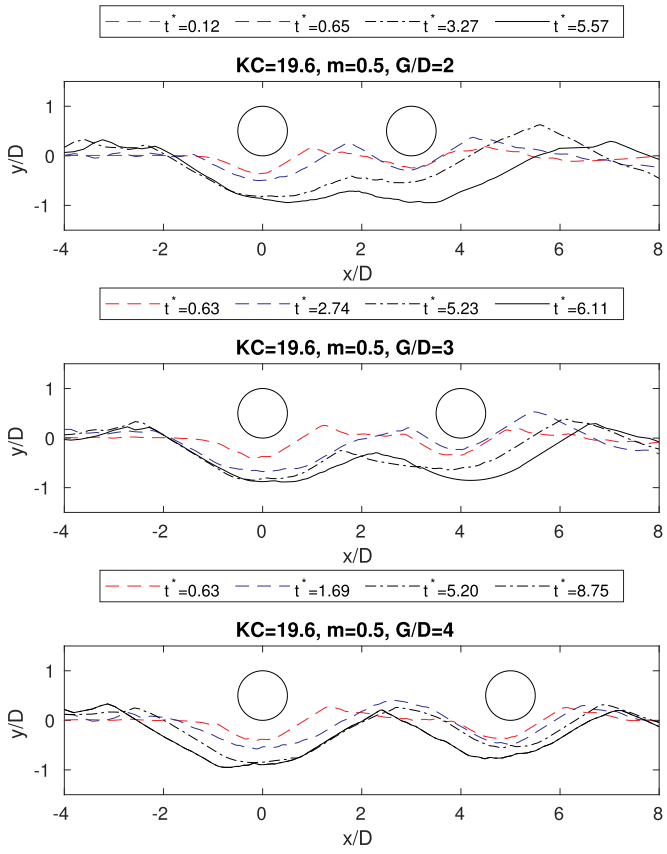

Fig. 15. Scour profile development with $KC = 19.6$, $m = 0.5$, $G/D = 2, 3$ and 4.

$$a_m = \begin{cases} 0.557 - 0.912(m - 0.25)^2, & 0 \le m \le 0.4 \\ -2.14m + 1.46, & 0.4 \le m \le 0.7 \end{cases} \tag{32}$$

$$b_m = \begin{cases} -1.14 + 2.24(m - 0.25)^2, & 0 \le m \le 0.4 \\ 3.3m - 2.5, & 0.4 \le m \le 0.7 \end{cases} \tag{33}$$

5.2.1. Pure-wave conditions $m = 0$

For a single pipeline in pure-wave conditions, the empirical equilibrium scour depth is a function of KC in the live-bed regime, i.e., $S_e/D = 0.1\sqrt{KC}$ (Sumer and Fredsøe, 1990), while for two tandem pipelines in pure waves the equilibrium scour depth must also potentially depend on the horizontal gap ratio G/D, i.e. such that:

$$\frac{S_e}{D} = f\left\{KC, \frac{G}{D}\right\} \tag{34}$$

It is seen in Fig. 19 that when $G/D = 1$ and 2, the trend in which the equilibrium scour depth for two tandem pipelines varies with KC is similar to that for single pipeline cases conducted by Larsen et al. (2016)

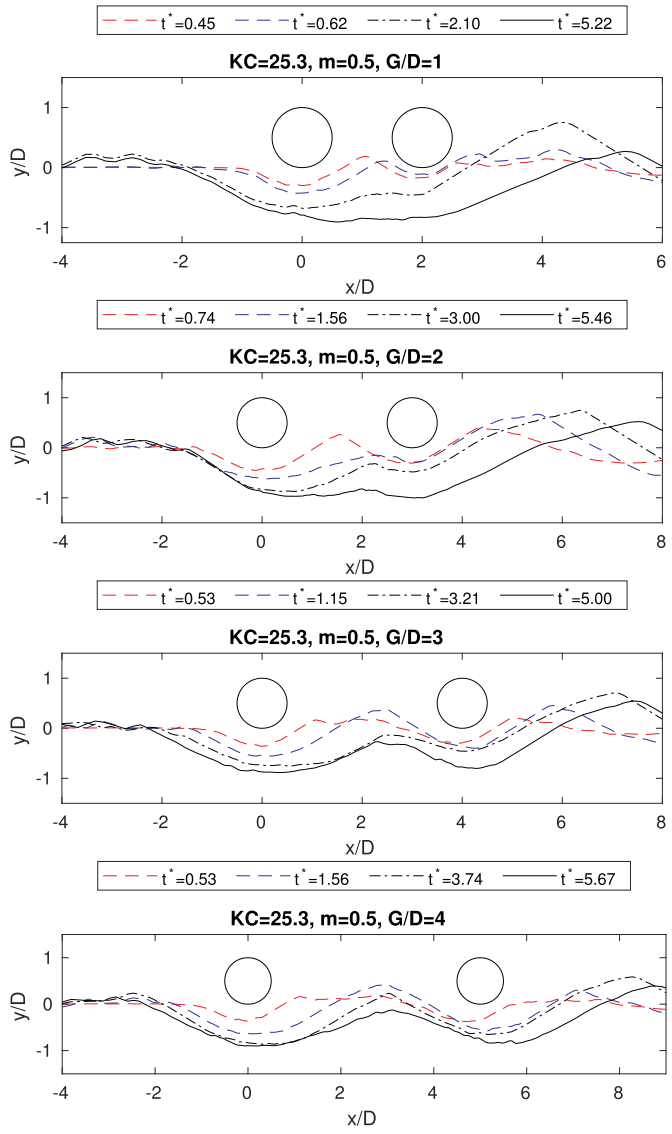

Fig. 16. Scour profile development with $KC = 25.3$, $m = 0.5$, $G/D = 1$, 2, 3 and 4.

but with a more significant drop in scour depth from $KC = 11$ to $KC = 15$. For $G/D = 3$ and 4, S_e/D increases with KC, which is in line with the trend of the empirical prediction for a single pipeline by Sumer and Fredsøe (1990).

For a given KC, the equilibrium scour depth generally increases with G/D. A special case is $KC = 11$, where the equilibrium scour depth with $KC = 11, G/D = 1$ is much higher than that with other KC at $G/D = 1$ and also higher than that with $KC = 11$ at other horizontal gap ratios. Similar phenomena were observed for a single pipeline with $KC = 11$ in simulations of Fuhrman et al. (2014) and Larsen et al. (2016). Fuhrman et al. (2014) explained the phenomenon as a resonance with the nature ripple length that is triggered within the model when KC is around 10–11. The profile develops a 'trough-to-trough' wavelength beneath the pipeline which closely matches with the nature length of vortex ripples. Therefore, the scour depth at around $KC = 10 - 11$ continually develops into a secondary stage and reached a final equilibrium. In Fig. 19, for $KC = 11$ the two dots in grey from Larsen et al. (2016) are the scour depths beneath a single pipeline at the first temporary equilibrium stage and the secondary equilibrium stage, respectively. In the present simulations, the equilibrium depth of $KC = 11$ at each horizontal gap ratio is dominated by the resonance phenomenon within the model so

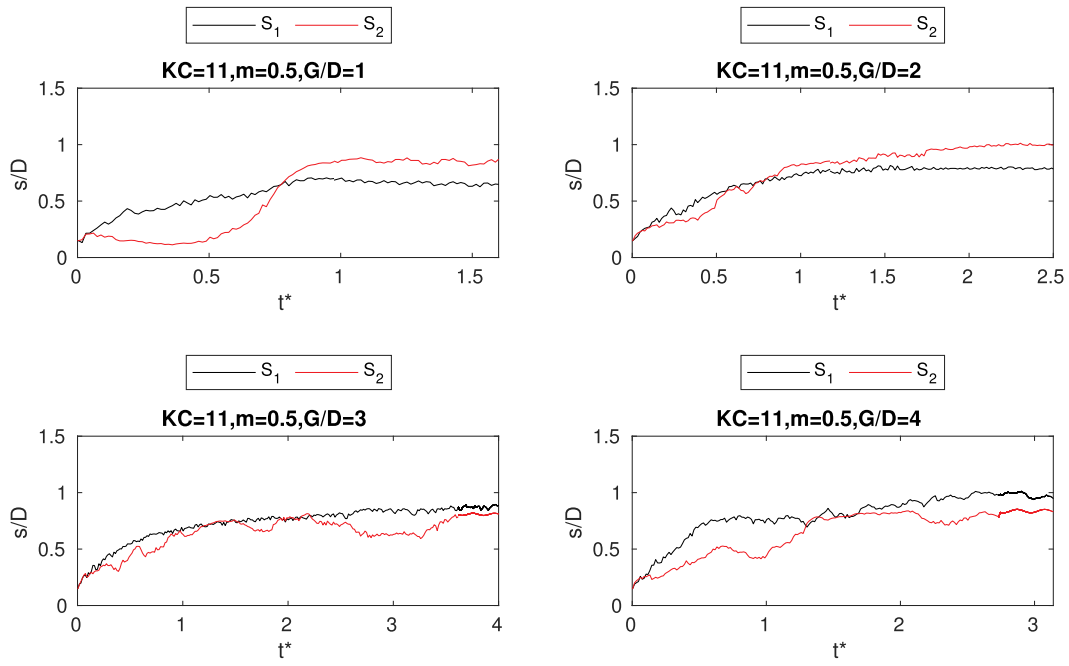

Fig. 17. Scour time series with $KC = 11$, $m = 0.5$.

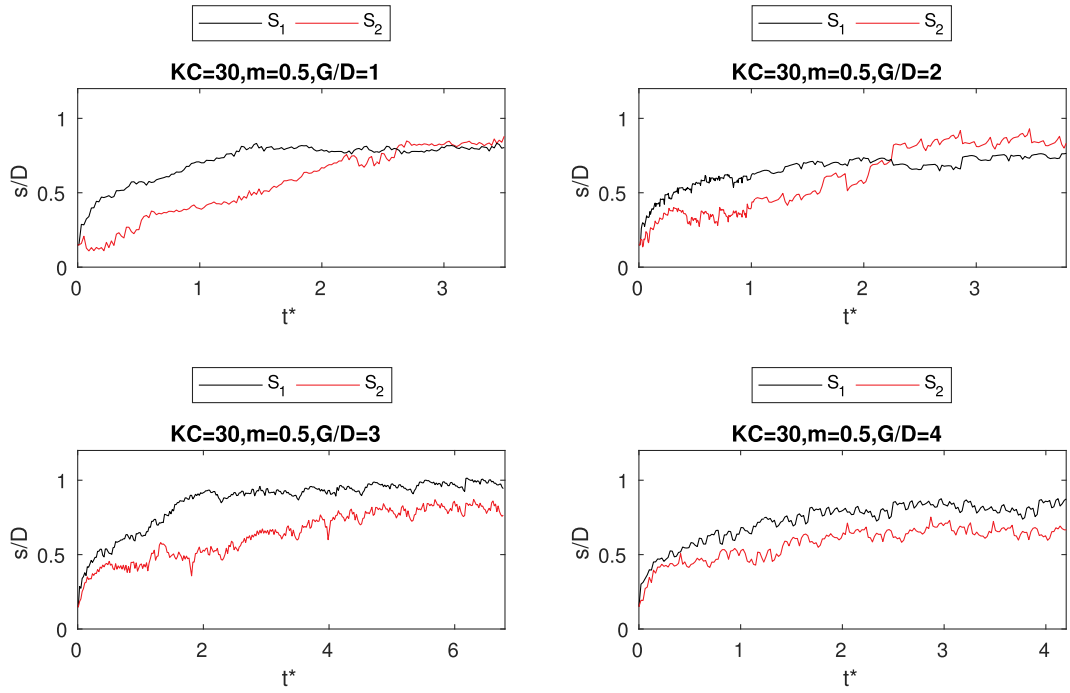

Fig. 18. Scour time series with $KC = 30$, $m = 0.5$.

that horizontal gap ratio has a relative small effect on $KC = 11$ compared to the other higher KC. It is worthwhile to mention that, in the present simulations, the equilibrium scour depths beneath two pipelines S_1 and S_2 are measured right below the center of the pipelines. The maximum scour depths in the scour hole may locate between two pipeline centers. Fig. 22 presents the scour profile with $KC = 11, G/D = 1, m = 0$. The averaged equilibrium scour depth S_e/D is 0.48, while the averaged maximum scour depth $S_{\max}/D$ is 0.625. In the study for a single pipeline in pure-waves by Larsen et al. (2016), the maximum scour depth locates right below the pipeline center, and the equilibrium scour depth is 0.62 at the secondary equilibrium stage. This explains why in Fig. 19, the S_e/D with $KC = 11$ for two pipelines is lower than that for a single pipeline from Larsen et al. (2016) while the equilibrium scour status for this specific case is dominated by the resonance phenomenon. It is noted that the equilibrium scour depths for $KC = 5.6$ also varies insignificantly with G/D, which will be explained later. It is emphasized that, while the resonance phenomenon discussed above can occur in numerical models, it has yet to be observed in physical experiments, to the best of the authors' knowledge.

For other KC (except for $KC = 5.6$ and 11), the equilibrium scour depth generally increases with G/D. For $G/D = 1$, the equilibrium scour depth beneath both pipelines is generally smaller than the empirical

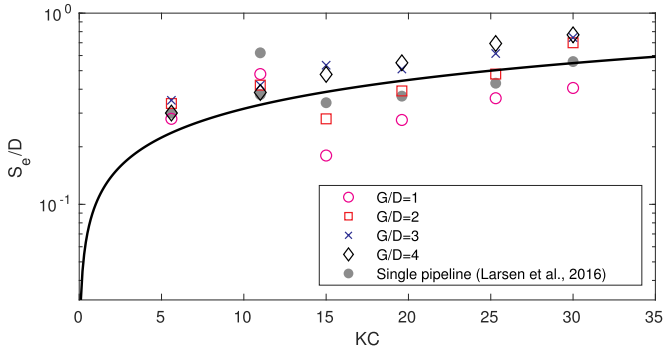

Fig. 19. Equilibrium scour depths beneath the centers of the upstream and downstream pipelines at $m = 0$. The solid reference line is the empirical solution for a single pipeline in waves (Sumer and Fredsøe, 1990), $S_e/D = 0.1\sqrt{KC}$.

prediction and also the simulation results (Larsen et al., 2016) for a single pipeline. The reduction of the scour depth with $G/D = 1$ can be explained by the suppression of the vortex shedding behind the upstream pipeline. The small spacing between the pipelines partially inhibits the shedding and further reduces the effect of the lee wake on the scour depth. It can be seen in Fig. 23a that for $KC = 19.6, G/D = 1, m = 0$, no vortex shedding occurs between two pipelines. As G/D increases to 2, vortex shedding begins to occur in the gap between two pipelines. However, the suppression of the vortex shedding will not happen for the $KC = 5.6$ case at $G/D = 1$. It is found that when $KC = 5.6$, the vortex shedding does not occur and the vortices remain attached to the pipelines during the half cycle of oscillating flow motions. Fig. 24 presents the computed velocity field (U) in the x direction with $KC = 5.6$ and $G/D = 1$ during the scouring process. Snapshots at three time instants are presented: just after a change in flow direction at $t/T = \frac{\pi}{8}$, at maximum velocity at $t/T = \frac{\pi}{2}$, and during deceleration of the flow prior to changing direction at $t/T = \frac{7\pi}{8}$. These show that for $KC = 5.6$ the vortex at the lee-side of the upstream pipeline does not reach the downstream pipeline before the flow changes its direction. The vortex at the lee-side of the downstream pipeline remains attached to the pipeline during the first half of the wave cycle. Similar phenomenon was presented in Sumer and Fredsøe (2006), i.e., vortex shedding does not occur when $KC = 4$ in the oscillating flows. This explains the results shown in Fig. 19, where the equilibrium scour depth computed with $KC = 5.6$ varies insignificantly with G/D ranging from 1 to 4. The equilibrium scour depth with $KC = 5.6$ is higher than the empirical predictions for a single pipeline but is consistent with the simulated result for a single pipeline in Larsen et al. (2016).

When the horizontal gap ratio increases to $G/D = 3$ and 4, the effect of KC is dominant. The equilibrium scour depths beneath two tandem pipelines are increased with KC in a similar way to the empirical prediction of scour beneath a single pipeline. It is seen in Fig. 19 that the equilibrium scour depths for $G/D = 3$ and 4 beneath two pipelines are generally higher than that beneath a single pipeline in Larsen et al. (2016). This is because of the mutual interaction of the lee-wake erosion from the upstream and the downstream pipelines in the oscillating flow. As can be seen in Figs. 23c and d that for $KC = 19.6, m = 0, G/D = 3$ and 4, vortices are shed from the upstream pipeline and interact with the downstream pipeline.

5.2.2. *Waves with weak current* $m = 0.25$

When the current of a relative strength $m = 0.25$ is added to the waves, the downstream pipeline can have a slightly higher equilibrium scour depth than the upstream pipeline, as shown in Fig. 20. The difference of the equilibrium scour depths between the upstream and the downstream pipelines is relatively obvious for $G/D = 2$ and 3. These differences can arise because the current-induced lee-wake vortex behind the upstream pipeline may influence the downstream pipeline, and this influence appears to be more apparent when $G/D = 2$ and 3. Detailed studies and reviews of the gap effect on the flow around two tandem cylinders in a current can be found in Zhou and Yiu (2006) and Sumner (2010). Zhou and Yiu (2006) have discussed that when the horizontal gap ratio between two cylinders is between 0 and 1, two cylinders in the current behave like a single 'extended-body' and no vortex shedding occurs in between. Once the gap between two pipelines exceeds a critical value of between 2 and 2.5 (Zhao et al., 2015), vortex shedding from the upstream cylinder will occur. The vortices shed from the pipeline will sweep the bed and amplify the shear stress and the sediment transport. Therefore, the scour depth at the downstream

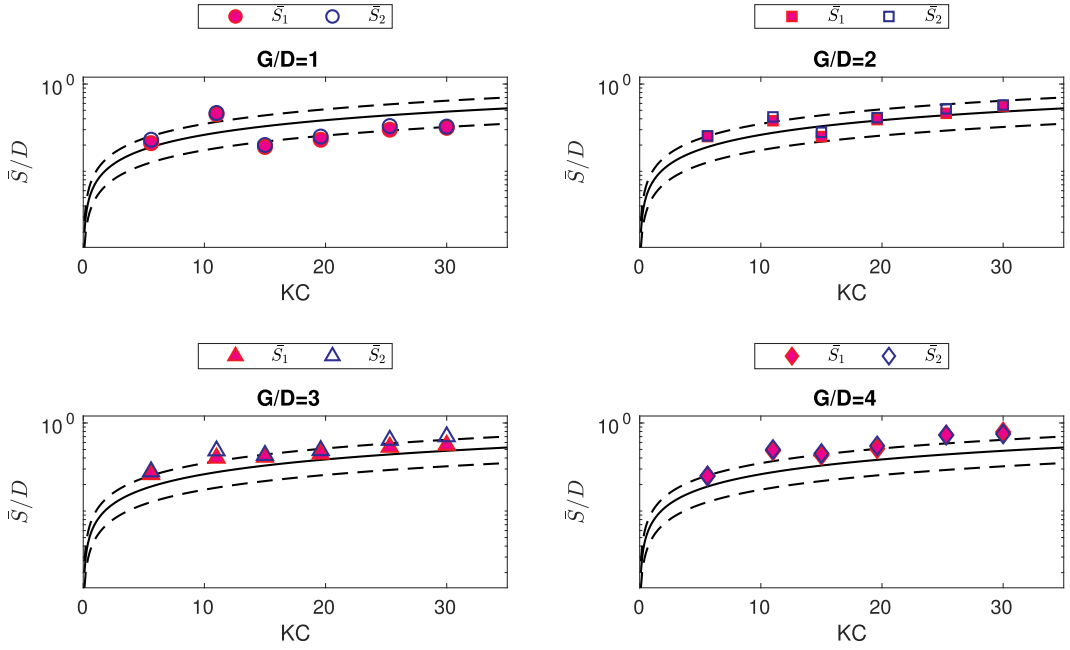

Fig. 20. Equilibrium scour depths beneath the centers of the upstream and downstream pipelines at $m = 0.25$. The solid reference line is the empirical solution for a single pipeline in combined waves and current (Sumer and Fredsøe, 1996). The dashed lines are the empirical solution with the standard deviation.

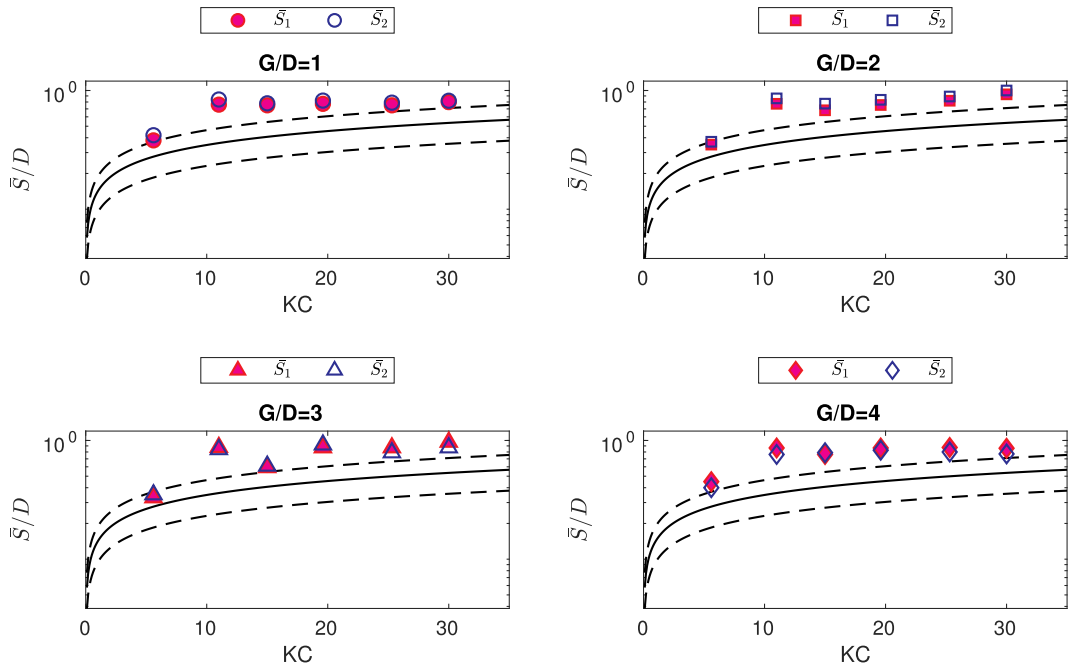

Fig. 21. Equilibrium scour depths beneath the centers of the upstream and downstream pipelines at $m = 0.5$. The solid reference line is the empirical solution for a single pipeline in combined waves and current (Sumer and Fredsøe, 1996). The dashed lines are the empirical solution with the standard deviation.

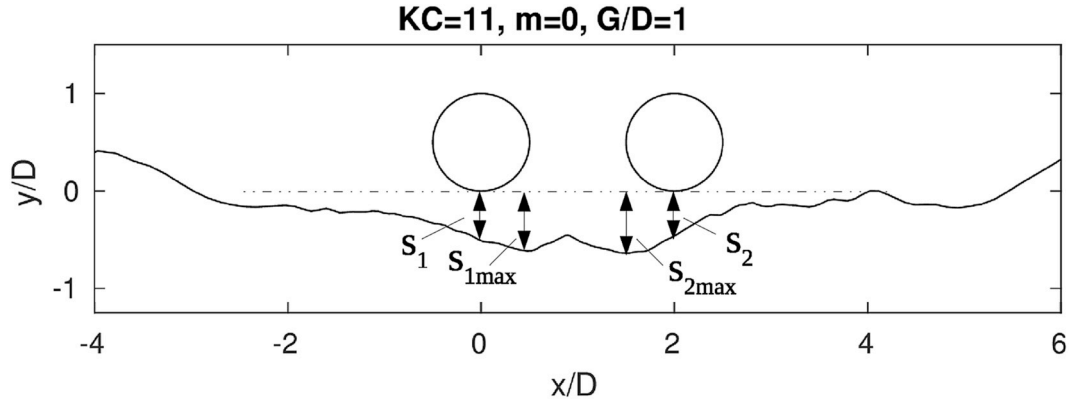

Fig. 22. Scour profile with $KC = 11, G/D = 1, m = 0$ after reaching equilibrium. The averaged scour depth beneath the pipelines is $S_e/D = (\overline{S_1}/D + \overline{S_2}/D)/2 = 0.48$. The averaged maximum scour depth between the pipelines is $S_{max}/D = (\overline{S_{1max}}/D + \overline{S_{2max}}/D)/2 = 0.625$. The equilibrium scour depth beneath a single pipeline with $KC = 11$ from Larsen et al. (2016) is $S/D = 0.62$.

pipeline is enhanced at the intermediate horizontal gap ratios. When G/D increases to 4, the influence from the vortex shedding behind the upstream pipeline on the downstream pipeline becomes less significant. The two pipelines then become more independent, so that at $G/D = 4$, the equilibrium scour depths beneath the upstream and downstream pipelines are very close to one another.

At each G/D, the trend of equilibrium scour depths varies with KC follows reasonably the empirical expression of Sumer and Fredsøe (1996). Furthermore, it is also worth noting that for $G/D = 1$ and 2, $m = 0.25$ in Fig. 20, the trend of equilibrium scour depths varies with KC is very similar to that for pure waves, i.e., $G/D = 1$ and 2, $m = 0$ in Fig. 19. Namely, a drop in scour depth from $KC = 11$ to $KC = 15$.

5.2.3. *Waves with strong current* $m = 0.5$

With $m = 0.5$, it appears in Fig. 21 that when KC is higher than 5.6, the equilibrium scour depth beneath the upstream pipeline is not affected by increases in KC. The equilibrium scour depths are generally located within the range of $S_e/D = 0.85 \pm 0.1$. Similarly, it was found in the experimental study of Sumer and Fredsøe (1996) that when there is a strong current combined with waves ($m > 0.7$ in their study), the equilibrium scour depth S_e/D is the same as in the current-alone case. As discussed before that when $m = 0.5$, the free stream flow behaves like a unidirectional current flow so that the results tend to be similar to those in pure-current conditions. Mao (1986) investigated the equilibrium scour depth versus Shields parameter in pure-current conditions, and it is found that when $\theta > 0.15$, the equilibrium scour depths are generally larger than those with $\theta < 0.15$ and are in the range of $S_e/D = 0.8 - 0.9$. As presented in Table 1, the far-field Shields parameters θ_{cw} with $m = 0.5$ for each KC exceed 0.15 except for $KC = 15$. The finding is consistent with the results in Larsen et al. (2016). Their simulation results of a single pipeline showed that for $KC = 11 - 30$ and $m \geq 0.5$, the equilibrium scour depths were slightly larger than the empirical solutions predicted by Eqn. (30)–(33), being close to the equilibrium scour depth in pure-current conditions, i.e. with $m = 1$.

Fig. 21 shows that the equilibrium scour depth beneath the downstream pipeline is higher than that beneath the upstream pipeline at $G/$

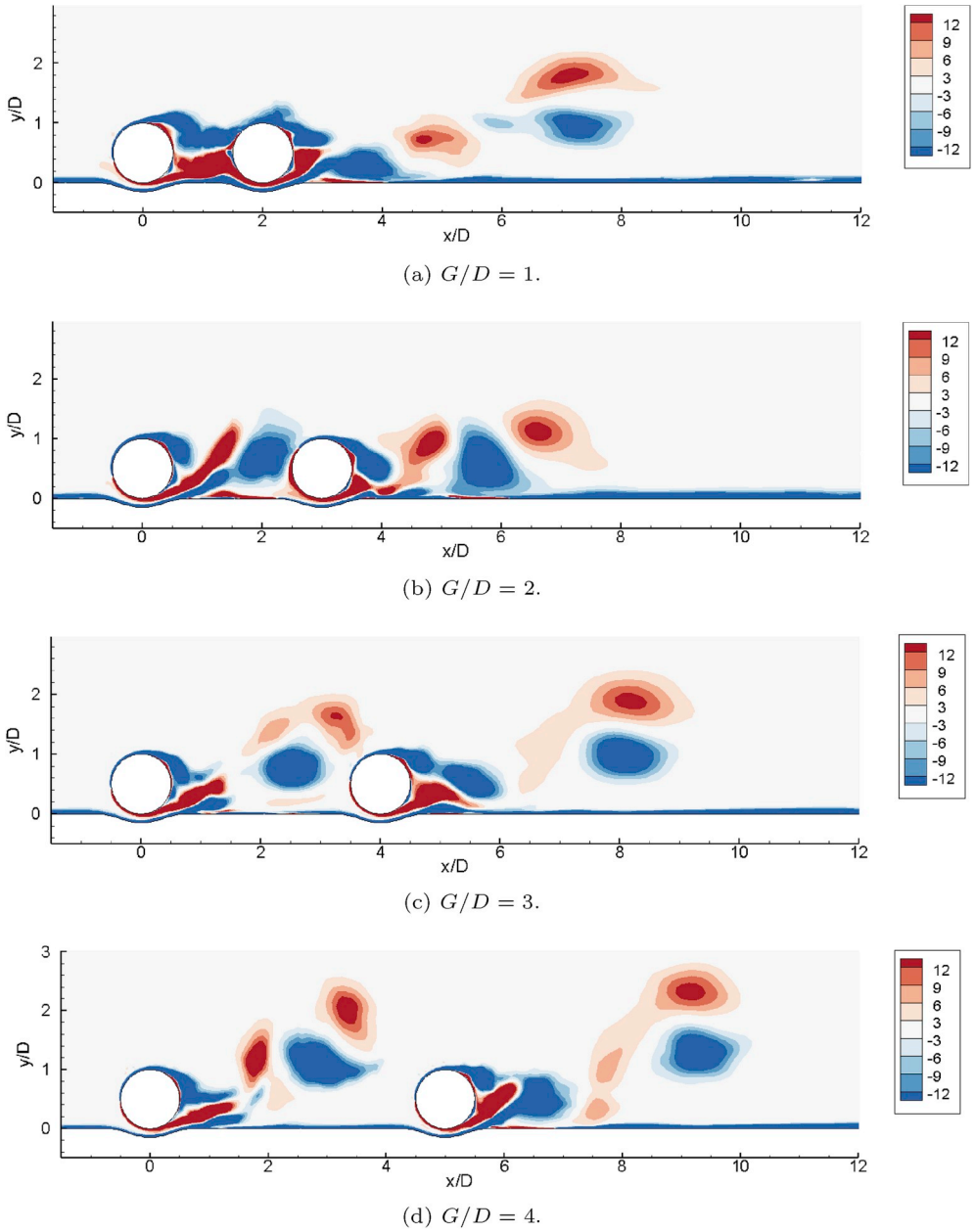

(a) $G/D = 1$.

(b) $G/D = 2$.

(c) $G/D = 3$.

(d) $G/D = 4$.

Fig. 23. Vorticity field (unit: $\frac{1}{s}$) of two pipelines in tandem with $KC = 19.6$, $m = 0$ at the maximum near-bed orbital velocity during the warm-up period (with morphology turned off).

$D = 2$. At $G/D = 3$ and 4, the present work finds that the upstream and downstream pipelines have nearly equivalent scour depths, while the downstream pipeline does not always have a higher equilibrium scour depth than the upstream pipeline. The finding is similar to the results of the experimental study on the scour beneath two tandem pipelines in pure-currents of Zhang et al. (2017).

6. Conclusions

The present study has investigated the local scour beneath two pipelines in tandem in the wave-plus-current conditions. A fully-coupled hydrodynamic and morphologic numerical model based on unsteady Reynolds-averaged Navier-Stokes (URANS) equations with k-ω turbulence closure has been applied. The model has been validated against existing experimental measurements of live-bed scour beneath a single pipeline (Mao, 1986) and as well as against experimental data involving live-bed scour beneath two pipelines in tandem (Zhao et al., 2015).

The scour profiles, scour time series and the equilibrium scour depths have been studied for two pipelines in tandem, with horizontal gap ratios ranging from 1 to 4, coupled with various KC and relative current strengths m. The following conclusions can be drawn from the present study.

- The effect of the Keulegan-Carpenter number, KC

The effect of KC on the scour beneath two pipelines is dominant when the current strength is low ($m = 0$ and 0.25) and the horizontal gap ratio is high ($G/D \geq 3$). The present study found that in such conditions, the trend in which the equilibrium scour depths for two tandem pipelines varies with KC is similar to that for a single pipeline: the equilibrium scour depth increases proportionally with $\sqrt{KC}$. When KC is small, e.g. $KC = 5.6$, vortex shedding does not occur because the wave period is small and the flows change direction prior to vortices being shed. Therefore, the horizontal gap ratio has a less significant influence

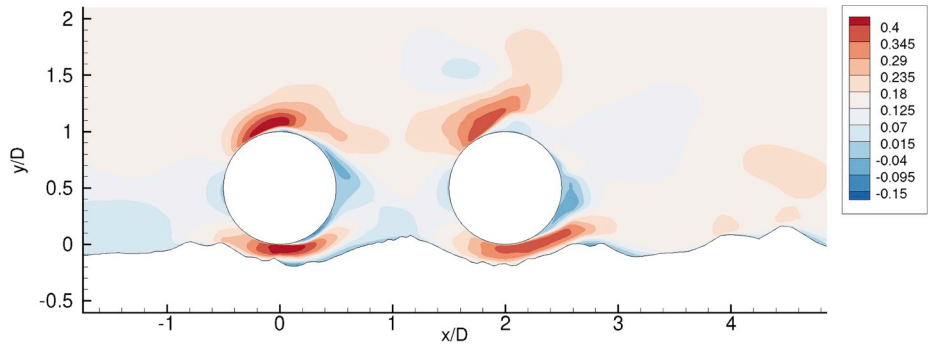

(a) $t/T = \frac{\pi}{8}$.

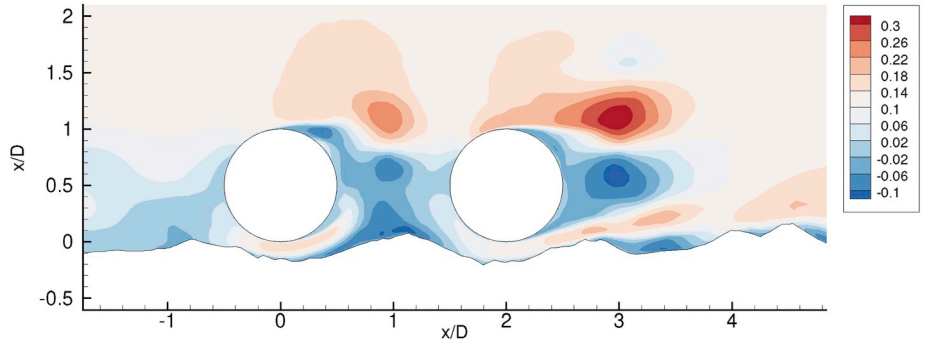

(b) $t/T = \frac{\pi}{2}$.

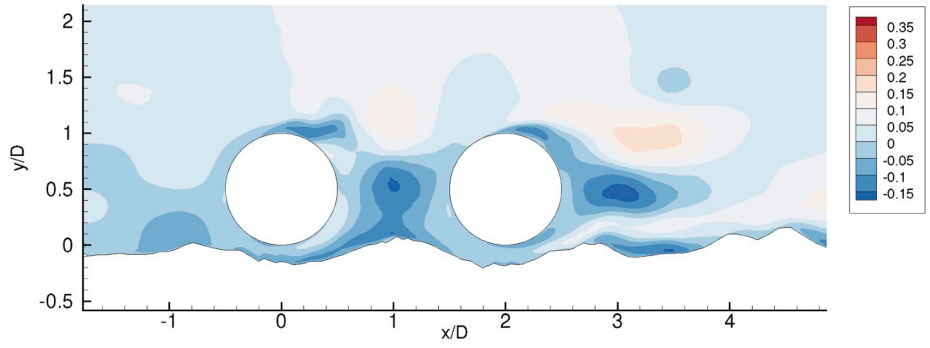

(c) $t/T = \frac{7\pi}{8}$.

Fig. 24. Horizontal velocity field u_x (unit: m/s) of two pipelines in tandem with $KC = 5.6$, $G/D = 1$, $m = 0$.

on the equilibrium scour depth. At a large horizontal gap ratio, i.e., $G/D = 4$ in the present study, KC also affects the number of berms that formed in between two pipelines in pure-wave conditions. When $KC \leq 15$, two or more berms are formed in the gap between two pipelines. With $m = 0.5$, KC has insignificant effect on the scour depth and the results tend to be similar to those in the pure-current conditions.

- The effect of the relative current strength, m

It is generally seen that with $m = 0$ and 0.25, the scour pattern is more similar to that in pure-wave conditions. With $m = 0.5$, the scour pattern is very similar to that in the pure-current conditions. With $m = 0$, i.e. pure-wave conditions, the time-averaged scour depth development is symmetric below the two tandem pipelines. At a relative high KC ($KC > 15$ in the present study), one berm is formed in between the two pipelines and the height of the berm gradually reduces during the scour process. However, it is still visible after reaching equilibrium for each horizontal gap ratio considered. The maximum scour depth is located in the gap between the two pipelines rather than below either of their respective centers. At a low current strength, the scour profiles still resemble those under pure-wave conditions, but with less symmetry. The downstream shoulder tends to be more eroded compared to pure-wave conditions. In waves plus strong-strength currents ($m = 0.5$), the flows effectively behave like a unidirectional current flow with a fluctuating "pumping" velocity from 0 to $2U_m$. Therefore, the scour pattern resembles that in pure current conditions. The scour depths are generally located in the range of $S_e/D = 0.85 \pm 0.1$ for the present cases. The scour beneath the downstream pipeline is delayed due to shielding from the upstream pipeline.

- The effect of the horizontal gap ratio, G/D

The present study shows that in pure-waves, when $G/D = 1$ the vortex shedding behind the upstream pipeline is suppressed, except for $KC = 5.6$, where vortex shedding does not occur. At a low relative current strength ($m = 0.25$), the scour depth beneath the downstream

pipeline is slightly higher than that upstream when $G/D = 2$ and 3, since that the current-induced lee-wake vortex behind the upstream pipeline will have the most effective influence on the downstream pipeline. At $G/D = 4$, the upstream pipeline and the downstream pipeline tend to have very similar equilibrium scour depths. Under strong currents ($m = 0.5$), when the horizontal gap ratio is small, i.e. $G/D = 1$ in the present study, the scour hole below the tandem pipelines will eventually merge to one since the two pipelines effectively behave like a single extended body. As the horizontal gap ratio increases, the two pipelines become more independent and essentially separate scour holes are formed. The present study found that a smaller horizontal gap ratio, i.e., $G/D = 1$, can cause a greater delay of the scour beneath the downstream pipeline with $m = 0.5$. It is also seen that with $m = 0.5$ the width of the scour hole beneath the upstream pipeline becomes larger as the horizontal gap ratio increases.

Declaration of competing interest

No conflict of interest.

Acknowledgment

This study was supported in part with computational resources provided by the Norwegian Metacenter for Computational Science (NOTUR), under Project No: NN9372K. The PhD project was financed by the Statoil Akademia program at the University of Stavanger.

References

Baykal, C., Sumer, B.M., Fuhrman, D.R., Jacobsen, N.G., Fredsøe, J., 2015. Numerical investigation of flow and scour around a vertical circular cylinder. Philos. Trans. R. Soc. A Math. Phys. Eng. Sci. 373, 20140104.
Bayraktar, D., Ahmad, J., Larsen, B.E., Carstensen, S., Fuhrman, D.R., 2016. Experimental and numerical study of wave-induced backfilling beneath submarine pipelines. Coast Eng. 118, 63–75.
Brøker, I.H., 1985. Wave Generated Ripples and Resulting Sediment Transport in Waves. Institute of Hydrodynamics and Hydraulic Engineering, Technical University of Denmark. Series paper No. 36.
Brørs, B., 1999. Numerical modeling of flow and scour at pipelines. J. Hydraul. Eng. 125, 511–523.
Cebeci, T., Chang, K., 1978. Calculation of incompressible rough-wall boundary-layer flows. AIAA J. 16, 730–735.
Chao, J., Hennessy, P., 1972. Local scour under ocean outfall pipelines. Journal 1443–1447.
Chiew, Y.-M., 1991. Prediction of maximum scour depth at submarine pipelines. J. Hydraul. Eng. 117, 452–466.
Engelund, F., Fredsøe, J., 1976. A sediment transport model for straight alluvial channels. Nord. Hydrol 7, 293–306.
Fredsøe, J., Deigaard, R., 1992. Mechanics of Coastal Sediment Transport, vol. 3. World scientific publishing company.
Fredsøe, J., Sumer, B.M., Arnskov, M., et al., 1991. Time scale for wave/current scour below pipelines. In: The First International Offshore and Polar Engineering Conference. International Society of Offshore and Polar Engineers.
Fuhrman, D.R., Baykal, C., Sumer, B.M., Jacobsen, N.G., Fredsøe, J., 2014. Numerical simulation of wave-induced scour and backfilling processes beneath submarine pipelines. Coast Eng. 94, 10–22.
Fuhrman, D.R., Schløer, S., Sterner, J., 2013. RANS-based simulation of turbulent wave boundary layer and sheet-flow sediment transport processes. Coast Eng. 73, 151–166.
Gao, F.-P., Han, X.-T., Cao, J., Sha, Y., Cui, J.-S., 2012. Submarine pipeline lateral instability on a sloping sandy seabed. Ocean Eng. 50, 44–52.
Hirschhausen, C., Gerbaulet, C., Kemfert, C., Lorenz, C., Oei, P.-Y., 2018. Energiewende "made in Germany" low carbon electricity sector reform in the European context: low carbon electricity sector reform in the European context. https://doi.org/10.1007/978-3-319-95126-3.
Jacobsen, N.G., 2011. A Full Hydro-And Morphodynamic Description of Breaker Bar Development (PhD thesis). Technical University of Denmark.
Jacobsen, N.G., Fredsoe, J., 2014. Formation and development of a breaker bar under regular waves. part 2: sediment transport and morphology. Coast Eng. 88, 55–68.
Larsen, B.E., Fuhrman, D.R., Baykal, C., Sumer, B.M., 2017. Tsunami-induced scour around monopile foundations. Coast Eng. 129, 36–49.
Larsen, B.E., Fuhrman, D.R., Sumer, B.M., 2016. Simulation of wave-plus-current scour beneath submarine pipelines. J. Waterw. Port, Coast. Ocean Eng. 142, 04016003.
Lee, C.-H., Low, Y.M., Chiew, Y.-M., 2016. Multi-dimensional rheology-based two-phase model for sediment transport and applications to sheet flow and pipeline scour. Phys. Fluids 28, 053305.
Li, F., Cheng, L., 1999. Numerical model for local scour under offshore pipelines. J. Hydraul. Eng. 125, 400–406.
Li, F., Cheng, L., 2000. Numerical simulation of pipeline local scour with lee-wake effects. Int. J. Offshore Polar Eng. 10.
Li, F., Cheng, L., 2001. Prediction of lee-wake scouring of pipelines in currents. J. Waterw. Port, Coast. Ocean Eng. 127, 106–112.
Liang, D., Cheng, L., 2005. Numerical model for wave-induced scour below a submarine pipeline. J. Waterw. Port, Coast. Ocean Eng. 131, 193–202.
Liang, D., Cheng, L., Li, F., 2005. Numerical modeling of flow and scour below a pipeline in currents: Part ii. scour simulation. Coast Eng. 52, 43–62.
Mao, Y., 1986. The Interaction between a Pipeline and an Erodible Bed (PhD thesis). Institute of Hydrodynamics and Hydraulic Engineering, Technical University of Denmark.
Marieu, V., Bonneton, P., Foster, D., Ardhuin, F., 2008. Modeling of vortex ripple morphodynamics. J. Geophys. Res.: Oceans 113.
Niemann, S., Fredsøe, J., Jacobsen, N.G., 2010. Sand dunes in steady flow at low froude numbers: dune height evolution and flow resistance. J. Hydraul. Eng. 137, 5–14.
Rijn, L.C.v., 1984. Sediment transport, part ii: suspended load transport. J. Hydraul. Eng. 110, 1613–1641.
Roulund, A., Sumer, B.M., Fredsøe, J., Michelsen, J., 2005. Numerical and experimental investigation of flow and scour around a circular pile. J. Fluid Mech. 534, 351–401.
Shi, Y.-M., Wang, N., Gao, F.-P., Qi, W.-G., Wang, J.-Q., 2019. Physical modeling of the axial pipe-soil interaction for pipeline walking on a sloping sandy seabed. Ocean Eng. 178, 20–30.
Soulsby, R., 1995. Bed shear-stresses due to combined waves and currents. Adv. Coast. Morphodynamics, 1995.
Sumer, B.M., 2007. Mathematical modelling of scour: a review. J. Hydraul. Res. 45, 723–735.
Sumer, B.M., 2014. A review of recent advances in numerical modelling of local scour problems. In: Proc., 7th Int. Conf. On Scour and Erosion, pp. 61–70.
Sumer, B.M., Fredsøe, J., 1990. Scour below pipelines in waves. J. Waterw. Port, Coast. Ocean Eng. 116, 307–323.
Sumer, B.M., Fredsøe, J., 1996. Scour Around Pipelines in Combined Waves and Current. Technical Report American Society of Mechanical Engineers, New York, NY (United States).
Sumer, B.M., Fredsøe, J., 2002. The Mechanics of Scour in the Marine Environment, vol.17. World Scientific Publishing Company.
Sumer, B.M., Fredsøe, J., 2006. Hydrodynamics Around Cylindrical Strucures, vol.26. World scientific.
Sumner, D., 2010. Two circular cylinders in cross-flow: a review. J. Fluids Struct. 26, 849–899.
Wilcox, D.C., 2006. Turbulence Modeling for CFD, third ed., vol. 2. DCW industries La Canada, CA.
Wilcox, D.C., 2008. Formulation of the k−ω turbulence model revisited. AIAA J. 46, 2823–2838.
Zhang, Q., Draper, S., Cheng, L., Zhao, M., An, H., 2017. Experimental study of local scour beneath two tandem pipelines in steady current. Coast Eng. J. 59, 1750002.
Zhao, M., Vaidya, S., Zhang, Q., Cheng, L., 2015. Local scour around two pipelines in tandem in steady current. Coast Eng. 98, 1–15.
Zhou, Y., Yiu, M., 2006. Flow structure, momentum and heat transport in a two-tandem-cylinder wake. J. Fluid Mech. 548, 17–48.